Journal of Geophysical Research: Solid Earth

RESEARCH ARTICLE
10.1029/2018JB015641

Tongji-Grace02s and Tongji-Grace02k: High-Precision Static GRACE-Only Global Earth's Gravity Field Models Derived by Refined Data Processing Strategies

Qiujie Chen[1,2,3], Yunzhong Shen[1], Olivier Francis[2], Wu Chen[3], Xingfu Zhang[4], and Houze Hsu[5]

[1]College of Surveying and Geo-informatics, Tongji University, Shanghai, China, [2]Faculté des Science, de la Technologie et de la Communication, University of Luxembourg, Luxembourg, Luxembourg, [3]Department of Land Surveying and Geo-informatics, The Hong Kong Polytechnic University, Hong Kong, [4]Departments of Surveying and Mapping, Guangdong University of Technology, Guangzhou, China, [5]State Key Laboratory of Geodesy and Earth's Dynamics, Institute of Geodesy and Geophysics, CAS, Wuhan, China

Key Points:
- Refined nongravitational acceleration modeling leads to improved gravity field solutions
- Superior static gravity field solutions Tongji-Grace02s and Tongji-Grace02k by enhancing data processing strategies were derived by refined data processing
- Sensitivity analyses of greatly reduced GRACE orbital altitude to gravity signals and contribution analyses of longer GRACE data series were analyzed

Correspondence to:
Y. Shen,
yzshen@tongji.edu.cn

Citation:
Chen, Q., Shen, Y., Francis, O., Chen, W., Zhang, X., & Hsu, H. (2018). Tongji-Grace02s and Tongji-Grace02k: High-precision static GRACE-only global Earth's gravity field models derived by refined data processing strategies. *Journal of Geophysical Research: Solid Earth*, *123*. https://doi.org/10.1029/2018JB015641

Received 11 SEP 2017
Accepted 18 JUN 2018
Accepted article online 26 JUN 2018

Abstract In order to derive high-precision static Gravity Recovery and Climate Experiment (GRACE)-only gravity field solutions, the following strategies were implemented in this study: (1) a refined accelerometer calibration model that treats monthly accelerometer scales as a third-order polynomial and daily accelerometer biases as a fifth-order polynomial was developed to calibrate accelerometer measurements; (2) the errors of the acceleration and attitude data were estimated together with the geopotential coefficients and accelerometer parameters on the basis of the weighted least squares adjustments; (3) a nearly complete observation series of GRACE mission was used to decrease the condition number of normal equation; and (4) the GRACE data collected in lower orbit altitude were also included to decrease the condition number. Our results show that (1) the refined accelerometer calibration model with much less parameters performs as well as previous methods (i.e., solving daily scales and hourly biases or estimating biases along with bias rates every 2 hr). However, it provides a system of more stable normal equation and less high-frequency noise in gravity field solutions; (2) high-frequency noise in the gravity field solution is reduced by modeling the errors of the acceleration and attitude data; (3) the geopotential coefficients at all degrees is greatly enhanced by using longer GRACE time series (especially the data by the end of 2010); and (4) due to lower orbit altitude, the GRACE data collected since 2014 lead to a significant improvement of the gravity field solution as the satellites are more sensitive to higher-frequency signal. Using the refined strategies, an unconstrained static solution (named Tongji-Grace02s) up to degree and order 180 was derived. For further suppressing the high-frequency noise, a regularization strategy based on the Kaula rule is applied to the degrees and orders beyond 80, leading to a regularized model Tongji-Grace02k. To validate the quality of the derived models, both Tongji-Grace02s and Tongji-Grace02k were compared to the latest GRACE-only models (i.e., GGM05S, ITU_GRACE16, ITSG-Grace2014s, and ITSG-Grace2014k) and validated using independent data (i.e., Global Navigation Satellite Systems (GNSS)/Leveling data and DTU13 oceanic gravity data). Compared to other models, much less spatial noise in terms of global gravity anomalies with respect to the state-of-the-art model EIGEN6C4 and far higher accuracy at high degrees are achieved by Tongji-Grace02s. The same conclusions can be drawn for Tongji-Grace02k when the same analyses were applied to the regularized solutions ITSG-Grace2014k and Tongji-Grace02k. Validations with independent data confirm that Tongji-Grace02s has the least noise among the unconstrained GRACE-only models and Tongji-Grace02k is the one with the best accuracy among the regularized GRACE-only solutions. For the tests up to degree and order 180 using GNSS/Leveling data, the improvements of Tongji-Grace02s with respect to ITSG-Grace2014s reach 13% over Canada and 23% in Mexico. Even better, no less than 58% of improvement is achieved by both Tongji-Grace02s relative to ITSG-Grace2014s and Tongji-Grace02k with respect to ITSG-Grace2014k in the validation based on DTU13 data.

1. Introduction

The Gravity Recovery and Climate Experiment (GRACE) mission jointly developed by the National Aeronautics and Space Administration (NASA) and the German Aerospace Center offered scientific information on both static and time-variable gravity fields of the Earth for almost 15 years (Kusche et al., 2012; Schmidt et al., 2006; Tapley et al., 2004). The GRACE mission consists of a pair of satellites separated about 200 km, tracking each other in a near-circular orbit of about 500-km altitude and 89.5° inclination. Both

satellites are equipped with accurate GNSS receivers for continuously measuring the satellites' orbits with a precision of a few centimeters and microwave ranging sensors for observing the intersatellite range rate with a higher accuracy of around 2 μm/s and SuperSTAR accelerometer sensors applied to observe the nongravitational acceleration with the accuracy level of 10^{-10}m/s^2 (Flury et al., 2008). The success of the GRACE mission basically depends on the orbit, intersatellite range rate, and accelerometer measurements. Based on the collected observations, a number of static GRACE-only gravity field models (e.g., ITG-GRACE2010 [Mayer-Gürr et al., 2010], AIUB-GRACE03S [Jäggi et al., 2010], GGM05S [Tapley et al., 2013], Tongji-GRACE01 [Chen, Shen, Zhang, Hsu, Chen, 2015; Chen, Shen, Zhang, Hsu, Chen, Ju, et al., 2015], ITSG-Grace2014s [Mayer-Gürr et al., 2014], ITSG-Grace2014k [Mayer-Gürr et al., 2014], ITU-GRACE16 [Guo et al., 2015], and HUST-Grace2016s [Zhou et al., 2017]) have been successfully derived by different data processing centers.

For static gravity field modeling, error sources originating from instrument errors (Chen et al., 2016; Klinger & Mayer-Gürr, 2016) and imperfect background force models (especially aliasing errors from ocean models and oceanic and atmospheric nontidal variation models; Kurtenbach et al., 2009; Seo et al., 2008) and orbit configuration (Dobslaw et al., 2016; Flechtner et al., 2016; Liu et al., 2010; Save, 2009) are generally recognized as the crucial factors affecting the quality of the estimated geopotential coefficients. As one of the most important error sources, the instrument errors caused by limited sensitivities of the sensors directly contaminate the primary GRACE observations (i.e., orbits, range rates, attitudes, and accelerations). The errors of the orbit measurements have a direct relation to the gravity field estimates (Ditmar et al., 2012; Zehentner & Mayer-Gürr, 2016), which can be suppressed by downweighting the orbit data during gravity field modeling (Bettadpur, 2012; Bruinsma et al., 2014; Dahle et al., 2012; Jäggiet al., 2010; Mayer-Gürr, 2006; Shen et al., 2015; Watkins & Yuan, 2014; Xu et al., 2017). Recently, low-frequency noise in the intersatellite range or range rate measurements has been demonstrated to contaminate the gravity field estimates; thus, either empirical parameters or covariance matrices are introduced to the intersatellite range or range rate data in various gravity field recovery methods (Behzadpour et al., 2016; Ditmar et al., 2012; Farahani et al., 2013; Liu et al., 2010; Zhao et al., 2011; Zhou et al., 2017).

In addition to the orbit and K-band ranging data errors, the errors of the accelerometer observations in the Scientific Reference Frame (SRF) measured by the accelerometers and the attitude data collected by the star cameras are also the important error sources in gravity field modeling. This is because the attitude data in terms of quaternion are directly applied to transform the accelerometer measurements from the SRF to the inertial frame. The transferred accelerometer data are employed for removing effects of atmospheric drag, solar radiation pressure, and the Earth albedo. The accelerometer device achieves the accuracies of 10^{-10} m/s^2 for two high sensitive axes (along-track and radial directions) and 10^{-9} m/s^2 for one less sensitive axis (Flury et al., 2008). The star camera has one boresight axis in *Z* direction and two cross-boresight axes in both *X* and *Y* directions (Bandikova & Flury, 2014; Inácio et al., 2015). As shown in Bandikova and Flury (2014) and Wu et al. (2006), the accuracies of the rotation across the boresight axes are almost 1 order of magnitude better than that along with the boresight one. Because of imperfectness of the sensors, both attitude and acceleration data are inevitably contaminated by measurement errors, which eventually degrade the derived gravity field models (Bandikova et al., 2014; Harvey, 2016). Bandikova et al. (2014) slightly improved the monthly gravity field solutions based on the attitude measurements reprocessed by combining the official SCA1B data and angular acceleration observations. As gravity field modeling directly relies on the quality of the accelerometer measurements, a data screening method for the accelerometer data was conducted by Klinger and Mayer-Gürr (2016). Other scientists (e.g., Flury et al., 2008; Inácio et al., 2015) also investigated the error behaviors of the attitude and accelerometer observations. As the quite important error sources in gravity field recovery, the errors of the attitude and acceleration data were estimated for the first time together with the geopotential coefficients and accelerometer parameters by using the weighted least squares method in Chen et al. (2016), which remarkably suppresses the high-frequency noise of the recovered monthly gravity field models. Although various stochastic models of errors in GRACE observables were employed by different research centers (Bettadpur, 2012; Dahle et al., 2012; Mayer-Gürr, 2006) in static GRACE-only gravity field modeling, both attitude and nongravitational acceleration corrections up to now are rarely estimated, which may amplify the noise at high degrees. In mathematical sense, considering the observation errors of the attitude and acceleration data in gravity field modeling is anticipated to derive a more stable normal equation.

The accelerometer measurements must be calibrated via scale and bias parameters before employed in gravity field recovery. Poor scale and bias estimates will certainly degrade orbit integration and eventually cause decrease of the quality of the gravity field solutions. Behaviors of both scales and biases to a great extent rely on thermal control service for the accelerometers (Klinger & Mayer-Gürr, 2016), which means that an accurate determination of gravity field models should consider the case when the thermal control service is switched off. In the past years, daily scales and hourly biases were generally applied to each accelerometer by a lot of data processing centers, for example, GeoForschungsZentrum Potsdam (Dahle et al., 2012) and Jet Propulsion Laboratory (JPL; Watkins & Yuan, 2014). Bonn University (Mayer-Gürr, 2006) and Tongji University (Chen, Shen, Zhang, Hsu, Chen, 2015; Chen, Shen, Zhang, Hsu, Chen, Ju, et al., 2015) even only solved the biases per hour. However, the accelerometers are probably impacted by temperature variations since April 2011 because the thermal control has been switched off since then, which means that the scales and biases for the accelerometer data may vary significantly (Klinger & Mayer-Gürr, 2016). Therefore, the processing methods should be updated so that the effects of the temperature variations of the accelerometers on gravity field recovery can be suppressed considerably. To consider the thermal variations, JPL introduced bias rate vectors for the accelerometer data in both X and Y components for the epochs after 2010 (Watkins & Yuan, 2014). Recent investigation conducted by Klinger and Mayer-Gürr (2016) reveals that estimating daily biases based on uniform cubic basis splines and daily scales based on fully populated scale factor matrices will dramatically reduce the impacts of the lack of the thermal control, and it even makes the C_{20} coefficients derived from the GRACE data become much closer to those solved from Satellite Laser Ranging data. Analogously, a low-order polynomial (3 order) for daily biases was introduced for each accelerometer in the along-track direction by Meyer et al. (2016), while only constant biases in both radial and cross-track directions were solved daily. Furthermore, a set of piecewise constant acceleration parameters in three axes of each accelerometer was estimated per 15 min so that the temperature changes of each accelerometer can be accounted for. Though the errors of accelerometer measurements of both satellites were solved in Chen et al. (2016), the accelerometer calibration method estimates accelerometer biases hourly for each accelerometer axis. This means that too many accelerometer parameters are required to be solved, which may lead to excessive parameterization. This study aims at deriving high-precision static GRACE-only gravity field models; thus, both scales and biases are modeled by polynomials besides estimating the errors of the attitude and acceleration data. Since the refined mathematical model in this paper reduces almost triple numbers of the accelerometer calibration parameters compared to that used in Chen et al. (2016) and estimates the attitude and acceleration errors, it is anticipated to create better conditioned normal equation and even lead to considerably enhanced static gravity field models.

As mentioned above, the GRACE orbit configuration is another crucial factor to prevent the improvement of gravity field estimation apart from the error sources from instruments. The twin GRACE satellites are flying in near-polar orbits, resulting in poor ground track coverage on both medium- and low-latitude regions. Consequently, the normal equations for global gravity field solutions are ill-conditioned (Save, 2009), which of course degrades gravity field models. Some simulation analyses (e.g., Bender et al., 2008; Dobslaw et al., 2016; Wiese, 2011) proved that adding a second pair of satellites with small orbit inclination will contribute more precise gravity field models, which substantially stabilizes the normal equation by improving the ground track coverage on the medium- and low-latitude areas. To reduce the impact of the sparse ground track coverage on the medium and low latitudes, one direct option is to use much longer GRACE data span in gravity field estimation, but ,currently even the high-quality model ITSG-Grace2014s only used the GRACE data in the time span February 2003 to December 2013. A sufficiently long GRACE data span, particularly including the data collected in significantly decreased orbital altitudes since 2014 (they show much stronger sensitivity to the gravity field signals), will be expected to remarkably improve the ill-conditioned normal equation and the gravity field estimates. Another option is applying regularization to the normal equation in deriving static gravity field solutions, which will markedly stabilize the ill-conditioned solutions as well. However, to our best of knowledge, until now only ITSG-Grace2014k from Graz University of Technology has been regularized based on the Kaula rule among the various static GRACE-only gravity field models released.

The main objectives of this study are to identify the error sources in static GRACE-only gravity field modeling and to develop refined data processing strategies for computing high-precision static GRACE-only gravity field models. In order to avoid excessive parameterization during calibrating accelerometer data, the

accelerometer scales and biases are modeled by polynomials. To account for the error sources from the observation errors, the errors of the orbit, intersatellite range rate, attitude, and accelerometer data are solved as well. The above strategies indeed are for deriving more stable normal equation, which is essential for the improvement of the gravity field estimates. To stabilize the recovered gravity field model, especially the high-degree coefficients, the GRACE-only data spanning the period January 2003 to July 2016 and a regularization method based on the Kaula rule are applied, leading to two high-precision static GRACE-only models (i.e., an unconstrained one called Tongji-Grace02s and a regularized one named Tongji-Grace02k). The rest of this paper is organized as follows. In section 2 a refined methodology for calibrating the accelerometer data in the SRF on the basis of Chen et al. (2016) and a regularized method based on the Kaula rule are presented. Detailed data processing for both unconstrained and regularized solutions is given in section 3. Section 4 discusses the benefit of the refined methodology and the added value of using long GRACE time series data and the contribution of the greatly decreased orbital altitudes since 2014. The analyses and verifications of the derived models are done in sections 5 and 6, respectively. Section 7 is left for concluding remarks.

2. Earth's Gravity Field Determination

The external potential of the Earth satisfies the Laplace equation. In general, the Earth's gravitational potential $V(r,\theta,\lambda)$ is expressed as follows (Heiskanen & Moritz, 1967):

$$V(r,\theta,\lambda)=\frac{GM_e}{r}\left[1+\sum_{n=2}^{\infty}\left(\frac{a_e}{r}\right)^n\sum_{m=0}^{n}\left(\overline{C}_{nm}\cos m\lambda+\overline{S}_{nm}\sin m\lambda\right)\overline{P}_{nm}(\cos\theta)\right] \tag{1}$$

where r,θ,λ are geocentric radius, colatitudes, and longitude at a particular location respectively; G stands for the gravitational constant; the factor M_e is the mass of the Earth, and a_e is the semimajor radius of the Earth; $\overline{P}_{nm}$ represents the normalized Legendre polynomial; and $\overline{C}_{nm}$ and $\overline{S}_{nm}$ denote geopotential coefficients to be estimated for degree n and order m. For GRACE-based gravity field modeling, the coefficients $\overline{C}_{nm}$ and $\overline{S}_{nm}$ up to degree and order N can be determined on the basis of the modified short-arc approach considering both attitude and accelerometer data errors (Chen et al., 2016). To avoid excessive parameterization in the accelerometer calibration model and reduce the impact of the ill-conditioned normal equation, this research further refines the methodology in Chen et al. (2016) via optimizing calibration model for both accelerometer biases and scales and applying regularization.

2.1. Review for the Method of Modeling Acceleration and Attitude Errors

The classical short-arc approach was applied to gravity field modeling by Mayer-Gürr (2006), while the errors of the accelerometer measurements and attitude observations were not considered. To account for these errors, Chen et al. (2016) introduced the corrections to the acceleration and attitude observations, leading to the linearized observation equations for the satellite's position and velocity vectors below:

$$\boldsymbol{r}(\tau_i)+\boldsymbol{v}_{\boldsymbol{r}}(\tau_i)=(\boldsymbol{r}_0+\boldsymbol{v}_{\boldsymbol{r}_0})(1-\tau_i)+(\boldsymbol{r}_N+\boldsymbol{v}_{\boldsymbol{r}_N})(\tau_i)-T^2\sum_{k=0}^{N}\alpha_k K_{\boldsymbol{r}}(\tau_i,\tau_k) \tag{2}$$

$$\left(\begin{array}{l}\boldsymbol{a}_g(\boldsymbol{r}_k,\boldsymbol{u}_0)+\boldsymbol{a}_{ng}\left(\boldsymbol{a}_s^k,\boldsymbol{q}^k,\boldsymbol{S}_0,\boldsymbol{b}_0\right)+\dfrac{\partial\boldsymbol{a}_g(\boldsymbol{r}_k,\boldsymbol{u}_0)}{\partial\boldsymbol{r}_k}\boldsymbol{v}_{\boldsymbol{r}_k}+\dfrac{\partial\boldsymbol{a}_g(\boldsymbol{r}_k,\boldsymbol{u}_0)}{\partial\boldsymbol{u}}\delta\boldsymbol{u}+\\ \dfrac{\partial\boldsymbol{a}_{ng}\left(\boldsymbol{a}_s^k,\boldsymbol{q}^k,\boldsymbol{S}_0,\boldsymbol{b}_0\right)}{\partial\boldsymbol{a}_s^k}\boldsymbol{v}_{\boldsymbol{a}_s^k}+\dfrac{\partial\boldsymbol{a}_{ng}\left(\boldsymbol{a}_s^k,\boldsymbol{q}^k,\boldsymbol{S}_0,\boldsymbol{b}_0\right)}{\partial\boldsymbol{q}^k}\boldsymbol{v}_{\boldsymbol{q}^k}+\dfrac{\partial\boldsymbol{a}_{ng}\left(\boldsymbol{a}_s^k,\boldsymbol{q}^k,\boldsymbol{S}_0,\boldsymbol{b}_0\right)}{\partial\boldsymbol{b}}\delta\boldsymbol{b}\end{array}\right)$$

$$\dot{\boldsymbol{r}}(\tau_i)=\frac{(\boldsymbol{r}_N+\upsilon_{r_N})-(\boldsymbol{r}_0+\upsilon_{r_o})}{T}+T\sum_{k=0}^{N}\beta_k\frac{\partial K_{\boldsymbol{r}}(\tau_i,\tau_k)}{\partial\tau_i} \tag{3}$$

$$\left(\begin{array}{l}\boldsymbol{a}_g(\boldsymbol{r}_k,\boldsymbol{u}_0)+\boldsymbol{a}_{ng}\left(\boldsymbol{a}_s^k,\boldsymbol{q}^k,\boldsymbol{S}_0,\boldsymbol{b}_0\right)+\dfrac{\partial\boldsymbol{a}_g(\boldsymbol{r}_k,\boldsymbol{u}_0)}{\partial\boldsymbol{r}_k}\boldsymbol{v}_{\boldsymbol{r}_k}+\dfrac{\partial\boldsymbol{a}_g(\boldsymbol{r}_k,\boldsymbol{u}_0)}{\partial\boldsymbol{u}}\delta\boldsymbol{u}+\\ \dfrac{\partial\boldsymbol{a}_{ng}\left(\boldsymbol{a}_s^k,\boldsymbol{q}^k,\boldsymbol{S}_0,\boldsymbol{b}_0\right)}{\partial\boldsymbol{a}_s^k}\boldsymbol{v}_{\boldsymbol{a}_s^k}+\dfrac{\partial\boldsymbol{a}_{ng}\left(\boldsymbol{a}_s^k,\boldsymbol{q}^k,\boldsymbol{S}_0,\boldsymbol{b}_0\right)}{\partial\boldsymbol{q}^k}\boldsymbol{v}_{\boldsymbol{q}^k}+\dfrac{\partial\boldsymbol{a}_{ng}\left(\boldsymbol{a}_s^k,\boldsymbol{q}^k,\boldsymbol{S}_0,\boldsymbol{b}_0\right)}{\partial\boldsymbol{b}}\delta\boldsymbol{b}\end{array}\right)$$

where $K_{\boldsymbol{r}}$ is the integral kernel defined in Mayer-Gürr (2006); T is arc length; α_k and β_k are integration coefficients; N is maximum index of epochs for each arc; $\boldsymbol{r}(\tau_k)(k=0,1,\ldots,N)$ and $\boldsymbol{v}_{\boldsymbol{r}}(\tau_k)(k=0,1,\ldots,N)$ stand for the satellite's position observations and the corresponding corrections at normalize time τ_k; the position

measurements at two boundaries of the arc, namely, $\boldsymbol{r}_0$and $\boldsymbol{r}_N$, are the special cases of $\boldsymbol{r}(\tau_k)$ when $k = 0$ and $k = N$; $\boldsymbol{v}_{\boldsymbol{a}_s^k}(k = 0, 1, \ldots, N)$ and $\boldsymbol{v}_{\boldsymbol{q}^k}(k = 0, 1, \ldots, N)$ are the corrections to the accelerometer measurements $\boldsymbol{a}_s^k$ $(k = 0, 1, \ldots, N)$ in the SRF and the attitude observations $\boldsymbol{q}^k(k = 0, 1, \ldots, N)$ respectively; and the scale vector $\boldsymbol{S}$ and bias vector $\boldsymbol{b}$ are used for calibrating the accelerometer observations $\boldsymbol{a}_s^k(k = 0, 1, \ldots, N)$. With the help of the attitude data $\boldsymbol{q}^k(k = 0, 1, \ldots, N)$, the calibrated accelerometer observations $\boldsymbol{a}_s^k(k = 0, 1, \ldots, N)$ are transformed from the SRF into the inertial frame according to $\boldsymbol{a_{ng}}(\boldsymbol{a_s}, \boldsymbol{q}, \boldsymbol{S}, \boldsymbol{b}) = \boldsymbol{C}(\boldsymbol{q})^{\boldsymbol{T}}(\boldsymbol{Sa_s} + \boldsymbol{b})$, in which the rotation matrix $\boldsymbol{C}(\boldsymbol{q})$ (from the inertial system to the SRF) is easily constructed by using the attitude observations in terms of quaternion $\boldsymbol{q} = (q_1 q_2 q_3 q_4)$. The gravitational acceleration $\boldsymbol{a}_g(k = 0, 1, \ldots, N)$ is associated with the satellite's position vector and gravity field parameters $\boldsymbol{u}$. The satellites' velocity vector $\dot{\boldsymbol{r}}(\tau_k)(k = 0, 1, \ldots, N)$ is expressed as a function regarding both gravitational acceleration and accelerometer data. $\boldsymbol{u_0}$ and $\boldsymbol{S_0}$ and $\boldsymbol{b_0}$ are a priori values of $\boldsymbol{u}$ and $\boldsymbol{S}$ and $\boldsymbol{b}$, respectively. To constrain the corrections to the attitude data, a linearized observation equation for the attitude observations is given as follows:

$$2\left(\boldsymbol{q}^i\right)^T \boldsymbol{v}_{\boldsymbol{q}^i} = 1 - \left(\boldsymbol{q}^i\right)^T \boldsymbol{q}^i \tag{4}$$

where the right-hand side may not be zero when data gaps occur and some interpolation methods are applied to interpolate every element in the missing quaternion data.

2.2. Gravity Field Modeling Based On Refined Accelerometer Calibration Method

Although the corrections to the accelerometer measurements and attitude observations in both equations (2) and (3) are applied to account for their observation errors in Chen et al. (2016), the accelerometer scales were only fixed by a priori values and the accelerometer biases were simply solved hourly, which may result in excessive parameterization. In this study, for each accelerometer axis, the biases are further modeled by using a *K*-order polynomial for each day and the scales are expressed as an *M*-order polynomial for each month:

$$\boldsymbol{b}(\tau_k) = d_0 + d_1(\tau_k - \tau_{\text{refb}}) + d_2(\tau_k - \tau_{\text{refb}})^2 + \ldots + d_K(\tau_k - \tau_{\text{refb}})^K \tag{5}$$

$$\boldsymbol{S}(\tau_k) = c_0 + c_1(\tau_k - \tau_{\text{refS}}) + c_2(\tau_k - \tau_{\text{refS}})^2 + \ldots + c_M(\tau_k - \tau_{\text{refS}})^M \tag{6}$$

where the scales and biases are both treated as time-dependent functions; τ_{refS} and τ_{refb} denote reference epochs for scales and biases, respectively; the polynomial coefficients for monthly scales $\boldsymbol{C} = (c_0, c_1, c_2, \ldots c_M)^{\boldsymbol{T}}$ and daily biases $\boldsymbol{D} = (d_0, d_1, d_2, \ldots d_K)^{\boldsymbol{T}}$ are parameters to be estimated. Implementing parameterization of monthly scales and daily biases in equations (5) and (6) and then substituting them into equations (2) and (3), the linearized observation equations (2) and (3) for the satellite's position and velocity vectors can be refined. Since the amount of the accelerometer parameters has been greatly reduced by only estimating the polynomial coefficients for monthly scales and daily biases, the normal equation is anticipated to be less ill-conditioned, which may lead to better gravity field estimates. To utilize the high-precision range rate measurement, the observation equation for the range rate measurement $\dot{\rho}(\tau_i)$ at the *i*-th epoch can be established as

$$\begin{aligned}\dot{\rho}(\tau_i) &= \boldsymbol{e}_{AB}^T(\tau_i)(\dot{\boldsymbol{r}}_B(\tau_i) - \dot{\boldsymbol{r}}_A(\tau_i)) \\ &= \boldsymbol{f}(\boldsymbol{r}_A(\tau_i), \boldsymbol{r}_B(\tau_i), \boldsymbol{a}_{s_A}, \boldsymbol{a}_{s_B}, \boldsymbol{q}_A, \boldsymbol{q}_B, \boldsymbol{u}, \boldsymbol{C}_A, \boldsymbol{C}_B, \boldsymbol{D}_A, \boldsymbol{D}_B)\end{aligned} \tag{7}$$

where the subscripts "*A*" and "*B*" denote the twin satellites GRACE A and GRACE B, respectively; $\boldsymbol{r}_A(\tau_i)$ and $\boldsymbol{r}_B(\tau_i)$ represent the position vectors for the twin satellites; and the velocity vectors for both satellites are denoted as $\dot{\boldsymbol{r}}_A(\tau_i)$ and $\dot{\boldsymbol{r}}_B(\tau_i)$ separately. Introducing a correction term $v_{\dot{\rho}}(\tau_i)$ to the range rate measurement at the *i*-th epoch and substituting the refined linearized observation equations for the satellite's position and velocity vectors into equation (7), we further conduct a linearized observation equation for the range rate

$$\begin{aligned}\dot{\rho}(\tau_i) \;+ v_{\dot{\rho}}(\tau_i) = \boldsymbol{f}(\boldsymbol{r}_A(\tau_i), \boldsymbol{r}_B(\tau_i), \boldsymbol{a}_{s_A}, \boldsymbol{a}_{s_B}, \boldsymbol{q}_A, \boldsymbol{q}_B, \boldsymbol{u}_0, \boldsymbol{C}_{A0}, \boldsymbol{C}_{B0}, \boldsymbol{D}_{A0}, \boldsymbol{D}_{B0}) + \frac{\partial \boldsymbol{f}}{\partial \boldsymbol{u}}\delta\boldsymbol{u} + \frac{\partial \boldsymbol{f}}{\partial \boldsymbol{C}_A}\delta\boldsymbol{C}_A + \frac{\partial \boldsymbol{f}}{\partial \boldsymbol{C}_B}\delta\boldsymbol{C}_B \\ + \frac{\partial \boldsymbol{f}}{\partial \boldsymbol{D}_A}\delta\boldsymbol{D}_A + \frac{\partial \boldsymbol{f}}{\partial \boldsymbol{D}_B}\delta\boldsymbol{D}_B + \sum_{k=0}^{N}\left(\frac{\partial \boldsymbol{f}}{\partial \boldsymbol{r}_{A_k}}v_{\boldsymbol{r}_{A_k}} + \frac{\partial \boldsymbol{f}}{\partial \boldsymbol{r}_{B_k}}v_{\boldsymbol{r}_{B_k}} + \frac{\partial \boldsymbol{f}}{\partial \boldsymbol{a}_{s_A}^k}v_{\boldsymbol{a}_{s_A}^k} + \frac{\partial \boldsymbol{f}}{\partial \boldsymbol{a}_{s_B}^k}v_{\boldsymbol{a}_{s_B}^k} + \frac{\partial \boldsymbol{f}}{\partial \boldsymbol{q}_A^k}v_{\boldsymbol{q}_A^k} + \frac{\partial \boldsymbol{f}}{\partial \boldsymbol{q}_B^k}v_{\boldsymbol{q}_B^k}\right)\end{aligned} \tag{8}$$

where $\delta\boldsymbol{C_A}$ and $\delta\boldsymbol{C_B}$ are the corrections to the polynomial coefficients of monthly scales; $\delta\boldsymbol{D_A}$ and $\delta\boldsymbol{D_B}$ stand for the corrections to the polynomial coefficients of daily biases; $\boldsymbol{v}_{r_A}$ and $\boldsymbol{v}_{r_B}$ are the orbit

correction vectors; and $\boldsymbol{e}_{AB}(\tau_i) = (\boldsymbol{r}_B(\tau_i) - \boldsymbol{r}_A(\tau_i))/\rho(\tau_i)$ is the unit vector of line-of-sight direction. For each arc, we rewrite the corrections to all parameters as $\boldsymbol{x}_j = \left(\delta\mu^T, \delta\boldsymbol{C}_A^T, \delta\boldsymbol{C}_B^T, \delta\boldsymbol{D}_A^T, \delta\boldsymbol{D}_B^T\right)^T$ and the correction vector to all the observations as $\boldsymbol{v}_j = \left(\boldsymbol{v}_{r_A}^T, \boldsymbol{v}_{r_B}^T, \boldsymbol{v}_{a_{s_A}}^T, \boldsymbol{v}_{a_{s_B}}^T, \boldsymbol{v}_{q_A}^T, \boldsymbol{v}_{q_B}^T, \boldsymbol{v}_{\dot{\rho}}^T\right)^T$. Based on the constraint equation to the attitudes and the observation equations for both the orbit positions and range rates that estimate polynomial coefficients $\boldsymbol{C}$ and $\boldsymbol{D}$, the partial derivative matrices $\boldsymbol{B}_{x_j}$ and $\boldsymbol{B}_{v_j}$ with respect to $\boldsymbol{x}_j$ and $\boldsymbol{v}_j$ respectively can be easily gathered along with the residual vector $\boldsymbol{y}_j$. Subsequently, the observation equations at the j-th arc can be simplified as

$$\boldsymbol{B}_{x_j}\boldsymbol{x}_j + \boldsymbol{B}_{v_j}\boldsymbol{v}_j = \boldsymbol{y}_j \tag{9}$$

Using a weight matrix $\boldsymbol{P}_j$ for all the observations (i.e., orbits, attitudes, and accelerations for both satellites and intersatellite range rates), the normal equation regarding all the parameters for each arc can be derived by minimizing $\boldsymbol{v}_j^T\boldsymbol{P}_j\boldsymbol{v}_j$ as follows:

$$\left(\boldsymbol{B}_{x_j}^T\left(\boldsymbol{B}_{v_j}\boldsymbol{P}_j^{-1}\boldsymbol{B}_{v_j}^T\right)^{-1}\boldsymbol{B}_{x_j}\right)\begin{pmatrix}\delta\boldsymbol{u}\\ \delta\boldsymbol{C}_A\\ \delta\boldsymbol{C}_B\\ \delta\boldsymbol{D}_A\\ \delta\boldsymbol{D}_B\end{pmatrix} = \boldsymbol{B}_{x_j}^T\left(\boldsymbol{B}_{v_j}\boldsymbol{P}_j^{-1}\boldsymbol{B}_{v_j}^T\right)^{-1}\boldsymbol{y}_j, j = 1, 2, \ldots, L \tag{10}$$

In an attempt to reduce the size of the final normal equation, the subnormal equations of all the arcs after eliminating the daily accelerometer biases are first merged. Then the monthly accelerometer scales are further eliminated from the merged normal equation, and consequently, a final unconstrained normal equation for solving the gravity field coefficients is conducted as follows:

$$\boldsymbol{N}_{uu}\delta\boldsymbol{u} = \boldsymbol{W}_u \tag{11}$$

where $\boldsymbol{N}_{uu}$ and $\boldsymbol{W}_u$ denote the normal matrix and the right-hand vector of the final normal equation. The least squares estimates of the geopotential coefficients can be directly computed with equation (11).

2.3. Regularized Gravity Field Solution

Due to the severely ill-conditioned normal equation, the coefficients of the unconstrained static gravity field model (especially at high degrees) are greatly contaminated by noise. With an attempt to reduce the noise, a regularized solution constrained by using the Kaula rule is briefly described in this section. If we define the regularization matrix based on the Kaula constraint as $\boldsymbol{K}$, then the regularized solution $\delta\boldsymbol{u}_\alpha$ can be obtained as follows:

$$\delta\boldsymbol{u}_\alpha = (\boldsymbol{N}_{uu} + \alpha\boldsymbol{K})^{-1}\boldsymbol{W}_u \tag{12}$$

where α is the regularization parameter. The regularized solution is biased, and the bias is evaluated by

$$\boldsymbol{b}_\alpha = -\alpha(\boldsymbol{N}_{uu} + \alpha\boldsymbol{K})^{-1}\boldsymbol{K}\overline{\delta\boldsymbol{u}} \tag{13}$$

where $\overline{\delta\mu}$ stands for the true geopotential coefficients. In practice, $\overline{\delta\mu}$ is usually replaced by the least squares solution. To determine the optimal regularization parameter, general cross-validation (GCV) method (Golub et al., 1979) is usually employed. If there are n observables in an ill-conditioned observational equation, the optimal regularization parameter determined by using the GCV approach is for ensuring that each observable can be best predicted by using the remaining $n - 1$ observables. However, this study prefers to use the mean square error (MSE) method (Shen et al., 2012) to determine the optimal regularization parameter, the reason for which will be discussed in section 3. The kernel of the MSE method is to keep a balance between noise reduction and bias caused by regularization. The MSE of the regularized solution is computed by

$$\mathrm{MSE}(\delta\boldsymbol{u}_\alpha) = \sigma_0^2\boldsymbol{Q}_\alpha\boldsymbol{N}_{uu}\boldsymbol{Q}_\alpha + \alpha^2\boldsymbol{Q}_\alpha\boldsymbol{K}\overline{\delta\boldsymbol{u}}\,\overline{\delta\boldsymbol{u}}^T\boldsymbol{K}\boldsymbol{Q}_\alpha \tag{14}$$

in which σ_0 is the variance of unit weight, $\mathbf{Q}_\alpha = (\mathbf{N_{uu}} + \alpha\mathbf{K})^{-1}$. In this investigation, the regularization parameter α is determined by minimizing the trace of MSE($\delta\boldsymbol{u}_\alpha$):

$$\min : \mathrm{trace}[\mathrm{MSE}(\delta\boldsymbol{u}_\alpha)] = \sigma_0^2\mathrm{trace}[\boldsymbol{Q}_\alpha\boldsymbol{N}_{\boldsymbol{uu}}\boldsymbol{Q}_\alpha] + \alpha^2\mathrm{trace}\left[\boldsymbol{Q}_\alpha\boldsymbol{K}\delta\boldsymbol{u}_L\delta\boldsymbol{u}_L^T\boldsymbol{K}\boldsymbol{Q}_\alpha\right] \tag{15}$$

where $\delta\boldsymbol{u}_L$ denotes the least squares solution.

3. Computation of Tongji-Grace02s and Tongji-Grace02k

3.1. Measurements

To develop high-precision static GRACE-based gravity field models, the GRACE Level-1B measurements (the acceleration and attitudes of the twin satellites and the intersatellite range rates) released by JPL for the period January 2003 to July 2016 are employed. Because the orbit data are sensitive to the geopotential coefficients at the very low degrees (Meyer et al., 2016) and the reduced-dynamic orbits from JPL are contaminated by a priori gravity field information (Jäggi et al., 2007), the reduced-dynamic orbits may lead to signal reductions of the solved gravity field models at the very low degrees. Hence, kinematic orbits (with the same data span as the applied official data) offered by Graz University of Technology are adopted instead of the reduced-dynamic ones used in Chen et al. (2016). However, the sampling rate for the kinematic orbits from Graz University of Technology is 10 s, which differs from the integration step (5 s) used in this study. Hence, the kinematic orbits are further interpolated to 5 s by using Lagrange interpolation method so as to be consistent with the integration step. The interpolated orbits, which are not directly determined by kinematic orbit determination techniques, are just for continuous orbit integration in the modified short-arc approach. To exclude the contributions from the interpolated orbits that are not directly determined by kinematic orbit determination techniques, their weights are set to zeros in forming the normal equation for gravity field solution. Since the kinematic orbits may contain outliers at some poor epochs, the outliers are detected in two steps. First, the kinematic orbits will be treated as outlier if the differences between the kinematic and reduced-dynamic orbits are larger than triple uncertainty of the kinematic orbits (about 4 cm; Zhao et al., 2011). Second, the outliers of the kinematic orbits are further identified if postfit residuals of the kinematic orbits exceed triple formal errors of the postfit residuals. In contrast to Chen et al. (2016), in order to incorporate various types of observations with different accuracies, the variance-covariance of the kinematic orbits from Graz University of Technology is applied for constructing the weight matrices together with the a priori accuracies of the intersatellite range rates, attitudes, and accelerations.

3.2. Gravitational and Nongravitational Accelerations

During orbit integration, the nongravitational and gravitational accelerations are calculated separately. Unlike the classical method that calibrates the nongravitational data by estimating daily scales and hourly biases for each accelerometer axis, an improved method estimating a 3-order polynomial for monthly accelerometer scales and a 5-order polynomial for daily accelerometer biases is used in this paper, whose benefits will be investigated in section 4. With an attempt to reduce iterative cost, a priori polynomial coefficients of the scales and biases are computed in two steps. First, the a priori scales and biases are calculated according to Bettadpur (2009). Second, the calculated scales and biases are used to estimate the a priori values of the polynomial coefficients for the scales and biases on the basis of the least squares method.

Regarding the gravitational acceleration, which is composed of mean gravity field, N-Body perturbations, general relativity effects, solid Earth (pole) tides, ocean (pole) tides, and atmospheric and oceanic dealiasing, some priori background force models as shown in Table 1 are applied. As the modified short-arc approach is insensitive toward prior gravity field information, EGM96 is sufficient to act as the mean gravity field in deriving both Tongji-Grace02s and Tongji-Grace02k. The N-Body perturbations, the general relativity effects, and the solid Earth (pole) tides are removed according to the IERS 2010 conventions. Regarding the oceanic tidal impacts, an ocean tide model named EOT11a containing 18 major tidal waves (Savcenko & Bosch, 2012) is applied to compute oceanic tidal corrections in terms of geopotential coefficients complete to degree and order 120. Based on the admittance theory by Rieser et al. (2012), 238 secondary waves are interpolated for further refinement of the oceanic tidal corrections. To account for the ocean pole tides and the atmospheric and oceanic dealiasing, the Desai model and the AOD1B Release 05 dealiasing products as listed in Table 1 are employed respectively.

Table 1
Summary of Force Models Used

Mean gravity field	EGM96 (Lemoine et al., 1998) up to degree/order 180
N-Body perturbations	Sun, Moon, and Jupiter (DE421 planetary ephemerides) (Folkner et al., 2008)
General relativistic effects	IERS 2010 conventions (Petit & Luzum, 2010)
Solid Earth (pole) tides	IERS 2010 conventions
Ocean Tides	EOT11a (Savcenko & Bosch, 2012) up to degree/order 120
Ocean Pole Tides	Desai model (Desai, 2002) complete to degree/order 30
Atmospheric and oceanic Dealiasing	AOD1B Release 05 de-aliasing products (Flechtner & Dobslaw, 2013) up to degree and order 100

3.3. Coefficients to Be Solved and Regularization

For the determination of the unconstrained static gravity field model Tongji-Grace02s, both global and local parameters as summarized in Table 2 are needed to estimate. To calibrate the accelerometer measurements, accelerometer scales and biases for each accelerometer axis are modeled by the monthly and daily polynomials, respectively. Regarding the global parameters, besides estimating the geopotential coefficients up to degree and order 180, trend and annual and semiannual terms are introduced for each geopotential coefficient below degree and order 50.

With the above parameters, the variations of coefficients $\boldsymbol{Var}(t)$ at low degrees are modeled as follows:

$$\boldsymbol{Var}(t) = \boldsymbol{trd}\frac{\Delta t}{365.25} + \boldsymbol{ap_1}\sin\left(\frac{2\pi\Delta t}{365.25} + \boldsymbol{ph_1}\right) + \boldsymbol{ap_2}\sin\left(\frac{\pi\Delta t}{365.25} + \boldsymbol{ph_2}\right) \tag{16}$$

where Δt is the difference between any time t(in unit of Modified Julian Day) and reference time (1 January 2005); $\boldsymbol{trd}$ stands for the trend; $\boldsymbol{ap}_1$ and $\boldsymbol{ap}_2$ denote the amplitudes for annual (365.25 days) and semiannual (365.25/2 days) variations respectively; and $\boldsymbol{ph}_1$ and $\boldsymbol{ph}_2$ are their corresponding phases. Nevertheless, the time-related parameters eventually are eliminated from the normal equation for the purpose of reducing the size of the final normal equation. Using the above data processing strategies, the final normal equation has been generated from a nearly complete observation series of the GRACE mission covering the period January 2003 to July 2016 (this is so far the longest time series among all the available GRACE-only static gravity field models) on the basis of the Satellite Gravimetry Analysis Software developed by Tongji University.

Here we show the eigenvalues of the unconstrained normal matrix for Tongji-Grace02s in terms of log10 in Figure 1, which indicates that the normal matrix is severely ill-conditioned (with condition number of 8.7×10^9). Directly solving the normal equation without any constraint or regularization produces an unconstrained gravity field solution entitled Tongji-Grace02s up to degree and order 180. To stabilize the ill-conditioned normal equation system caused by poorer sensitivity of the GRACE mission to high-frequency signal (approximately above degree 80) compared to the Gravity Field and Steady State Ocean Circulation Explorer (GOCE; Pail et al., 2010), a regularization matrix constructed by using the Kaula rule for the degrees ranging 81 to 180 is further applied. Once the regularization matrix has been constructed, the optimal regularization factor for the normal matrix can be obtained on the basis of either the MSE or GCV method. Following the MSE and GCV approaches, we respectively present the traces of MSE and GCV in terms of log10 in Figures 2a and 2b for various regularization parameters. In Figures 2a and 2b, we can find that the MSE method suggests that the optimal regularization factor is 2.0×10^7 as indicated by a red dot in

Table 2
Summary of Parameters in Unconstrained Gravity Field Modeling

Parameter type	Description	Parameter period
Local	Scales (5-order polynomial per accelerometer axis)	One month
	Biases (3-order polynomial per accelerometer axis)	One day
Global	Geopotential coefficients (degree/order 180)	Until the end
	Trend, annual, and semiannual terms (degree/order 50)	Until the end

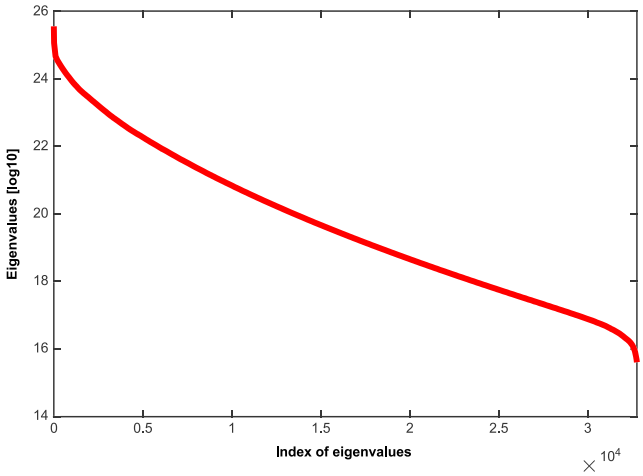

Figure 1. Eigenvalues of the unconstrained normal matrix for Tongji-Grace02s.

Figure 2a, while another optimal one achieved by using the GCV approach turns out to be 9.0×10^6 as marked by a black circle in Figure 2b. The difference of the optimal regularization factors between the MSE and GCV methods is relatively small, whose impact on gravity field estimates will be further discussed latter. As mentioned above, the regularized gravity field model in practice is a biased solution and the bias is a function of the regularization factor. According to the second term in the right hand of equation (14), the traces of MSEs from the regularization biases for varying regularization factors are depicted in Figure 2c. We can see from Figure 2c that the regularization bias increases with regularization factor, which means that the optimal regularization factor is for keeping a balance between noise reduction of the solved gravity field model and bias increase caused by the regularization.

In order to discuss the impact of the discrepancy between the two regularization methods, the optimal regularization factors based on both regularization methods are applied to infer regularized static gravity field models on the basis of our normal equation. To comprehensively discuss the spectrums of the estimated geopotential coefficients of the derived models, geoid degree heights of the derived models with respect to a high-quality reference gravity field model are usually computed by

$$\sigma_n = a_e \sqrt{\sum_{m=0}^{n} \left(\left(C_{nm} - C_{nm}^{ref}\right)^2 + \left(S_{nm} - S_{nm}^{ref}\right)^2 \right)} \tag{17}$$

where the coefficients C_{nm}^{ref} and S_{nm}^{ref} are from EIGEN6C4 (Förste et al., 2014), a high-quality combined gravity field model computed by taking terrestrial measurements and multi-LEO satellites' data into account, consisting of GRACE, GOCE (Drinkwater et al., 2006), and Laser Geodynamics Satellite (LAGEOS) (Diedrich & Gendt, 1989); a_e is the semimajor radius of the Earth. Note that the coefficients of the combined model at low degrees (especially below degree 40) are generally dominated by the GRACE data and remaining unmodeled time-variable signals. They also vary when different reference epochs are used in modeling the variations in low-degree coefficients. Therefore, the geoid degree heights at the low degrees (especially below degree 40) just reveal how well they fit between the solved gravity field models and the reference one. Nevertheless, the geoid degree heights at the high degrees relative to the state-of-the-art reference model can be regarded as noise level of the derived gravity field solution at the high degrees because that the coefficients of the combined solutions at the high degrees are dominated by the measurements of the GOCE gradients and terrestrial data, which show much stronger sensitivity to the gravity field signals at the high degrees.

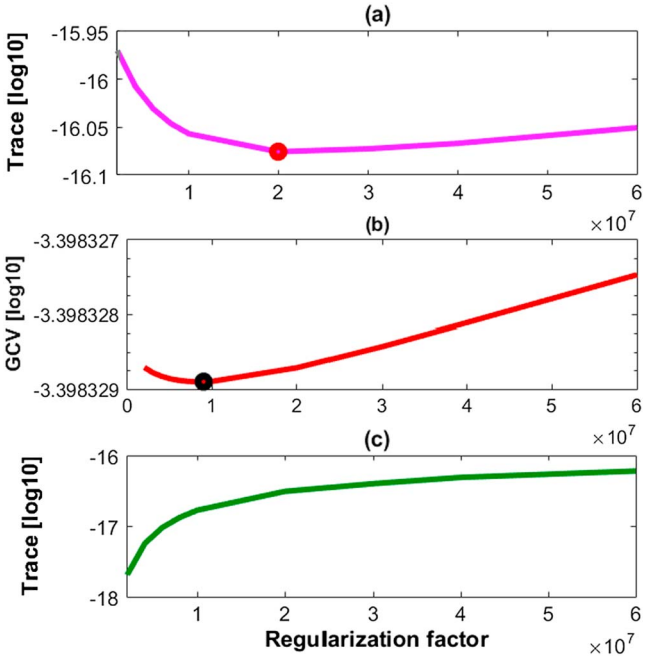

Figure 2. Trace of (a) MSE and (b) GCV, as well as (c) trace of regularization bias.

According to equation (17), the geoid degree heights of the two regularized models and the unconstrained solution are presented in Figure 3. It demonstrates that both GCV and MSE techniques can achieve noise reduction at the high degrees in addition to retaining the consistent signals at the low and medium degrees as the unconstrained solution. Considering a slight reduction of noise contributed by the MSE method for the degrees over 160, we propose to use the MSE method for regularization in deriving Tongji-Grace02k.

4. Benefits of the Refined Data Processing Strategies

Two of the key efforts for improving gravity field solution we have done in this research are (1) estimating the observation errors of both the accelerations and attitudes and (2) further improving the calibration model for the

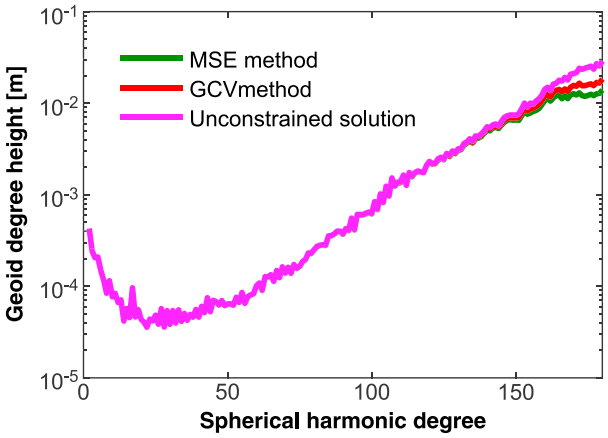

Figure 3. Contributions from the MSE and GCV approaches.

accelerometer scales and biases, in which an *M*-order polynomial for the monthly scales and a *K*-order polynomial for the daily biases are estimated together with the geopotential coefficients via the weighted least squares adjustment. The contributions of these two efforts to gravity field estimates are discussed in detail here.

4.1. Determination of Polynomials for Accelerometer Scales and Biases

Before evaluating the improvements contributed by the refined nongravitational acceleration modeling, we first design six cases (from A to F) for gravity field recovery as shown in Table 3 to determine the reasonable orders for the polynomials of the monthly scales and daily biases. The data used in these cases are from the GRACE observations in August 2014 since the thermal control of the GRACE mission in this month was switched off. Following the cases and the given data, six gravity field models up to degree and order 80 are computed. The comparisons among the six models in terms of geoid degree height with respect to EIGEN6C4 are presented in Figures 4a and 4b. From Figures 4a and 4b we find that (a) when the order of the daily polynomial for accelerometer biases is fixed by 5, a 3-order polynomial for the monthly accelerometer scales can derive the best solution and (b) once the order of the polynomial for the monthly scales is set to 3, a polynomial with 5 order for the daily biases is the appropriate choice in Figure 4b. Hence, this paper uses 3-order and 5-order polynomials to model the monthly scales and daily biases, respectively.

To investigate the temporal variations of the scale and bias estimates, monthly mean values are subtracted from the scale and bias estimates for the month August 2014. The resulting residuals of both scales and biases are displayed in Figures 5a–5c and 5g–5i, which show that both scales and biases in *Y* and *Z* axes experience significant daily variations (especially the linear and quadratic changes), while the variations in *X* direction are not obvious. Similarly, we plot the discrepancies between the accelerometer estimates and the daily mean values in Figures 5d–5f for scales and Figures 5j–5l for biases, respectively. It can be well observed that the residuals of both scales and biases (in *Y* and *Z* directions) after subtracting daily mean values are also dominated by linear variations. These linear variations in daily scale differences are expected to be absorbed by the low-order terms of the polynomial used in monthly scale modeling, while the linear variations in daily bias differences are anticipated to be compensated by the linear terms of the polynomial used in daily bias estimation. To confirm the above statement, Figure 6 presents the scale residuals after removing linear and quadratic terms from the monthly scale estimates and the bias residuals after subtracting linear terms from the daily bias estimates. It clearly shows that the daily linear variations almost disappear, demonstrating that the low-order terms of the polynomials used in estimating monthly scales and daily biases can compensate most of the daily linear variations in both scales and biases. We also show the standard deviation values of the discrepancies of the accelerometer estimates with respect to the monthly and daily mean values and the dominant estimates from low-order terms of the polynomials, which are given in Table 4. It reveals that the residuals computed by subtracting the linear terms from daily biases and removing both linear and quadratic terms from monthly scales achieve the smallest standard deviations. This finding demonstrates the feasibilities of the polynomials employed in daily bias estimation and monthly scale modeling to compensate the temporal variations in accelerometer scales and biases.

Table 3
Cases for Gravity Field Modeling

Case	Errors of accelerations and attitudes	Scales		Biases	
		Period	Polynomial	Period	Polynomial
A	estimated	One month	1 order	daily	5 order
B	estimated	One month	3 order	daily	5 order
C	estimated	One month	5 order	daily	5 order
D	estimated	One month	7 order	daily	5 order
E	estimated	One month	3 order	daily	4 order
F	estimated	One month	3 order	daily	6 order

4.2. Analyses of the Nongravitational Acceleration Modeling Method

For more comparisons, we design two more cases (i.e., G and H) in Table 5 to generate gravity field models up to degree and order 80 from the GRACE data as used in section 4.1. Case G is the classical approach, and case H is recently used by JPL to consider the possible linear variations in the accelerometer biases (Watkins & Yuan, 2014). Both cases G and H estimate the errors of acceleration and attitude data and solve the accelerometer scales per day. The difference is that the accelerometer biases are solved per hour in the case G, while the scheme H estimates accelerometer

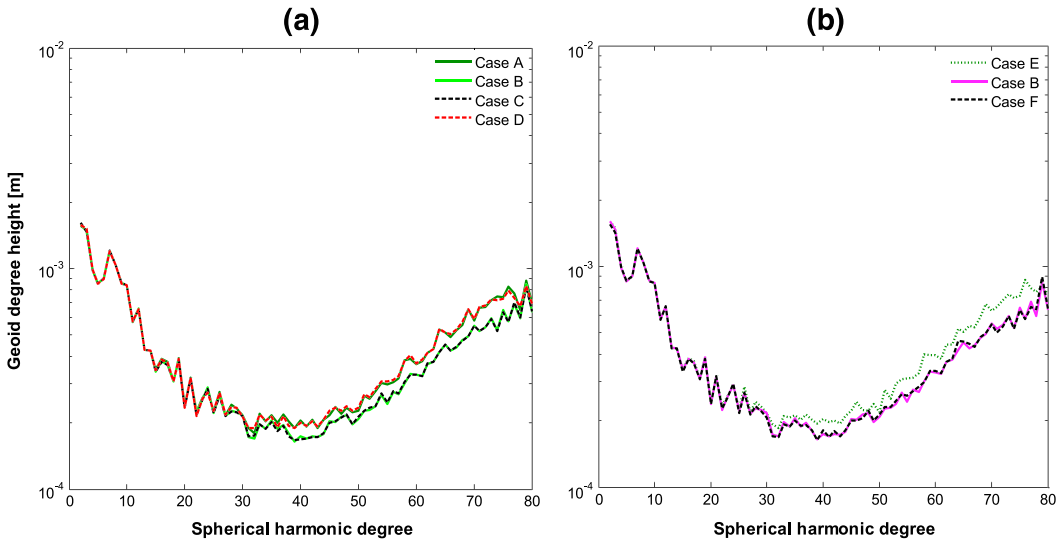

Figure 4. (a) Selection of accelerometer scales and (b) selection of accelerometer biases.

bias rates besides solving biases each 2 hr. Subsequently, the accelerometer scales and biases solved by using the cases B and G and H for the month August 2014 are plotted in Figure 7 and the statistics of the differences of case B with respect to cases G and H are given in Table 6. Figure 7 and Table 6 demonstrate that both scales and biases derived from case B generally show a good agreement with those from cases G and H. Although the standard deviations of case B relative to the other two cases show larger differences in *Y* direction for both scales and biases, which are caused by the relatively larger scales and biases in *Y* axis, the standard deviations have a magnitude of 1×10^{-9} m/s^2 for biases and a magnitude of 1×10^{-3} for scales in both *X* and *Z* directions.

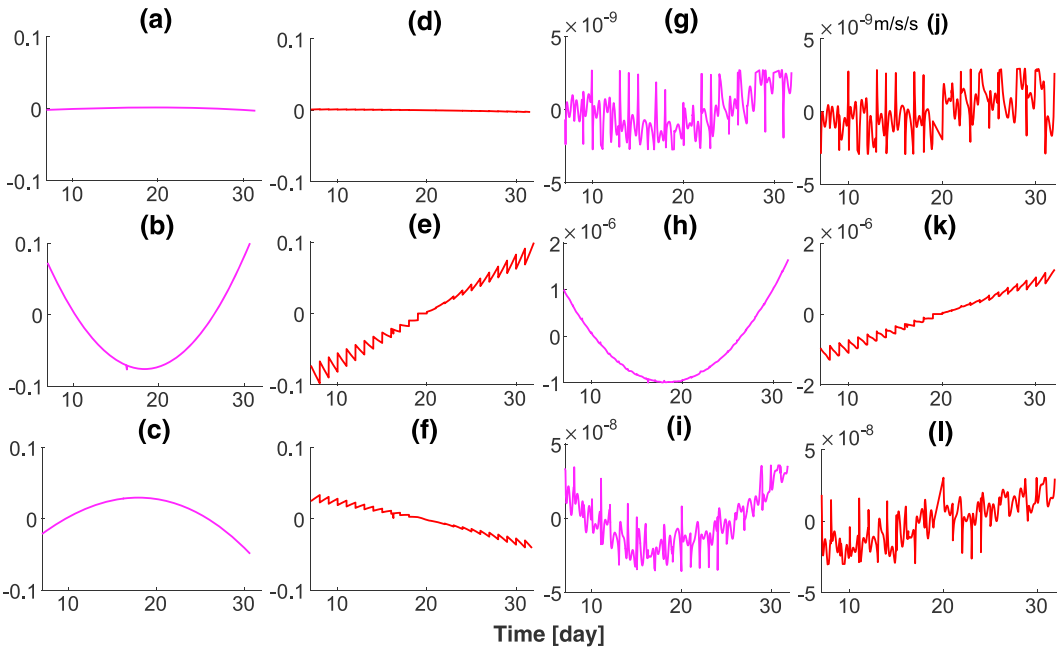

Figure 5. (a–c) Accelerometer scales minus monthly mean scales in *X*, *Y*, and *Z* axes; (d–f) accelerometer scales minus daily mean scales in *X*, *Y*, and *Z* directions; (g–i) differences between accelerometer biases and monthly mean biases in *X*, *Y*, and *Z* axes; and (j–l) differences between accelerometer biases and daily mean biases in *X*, *Y*, and *Z* directions.

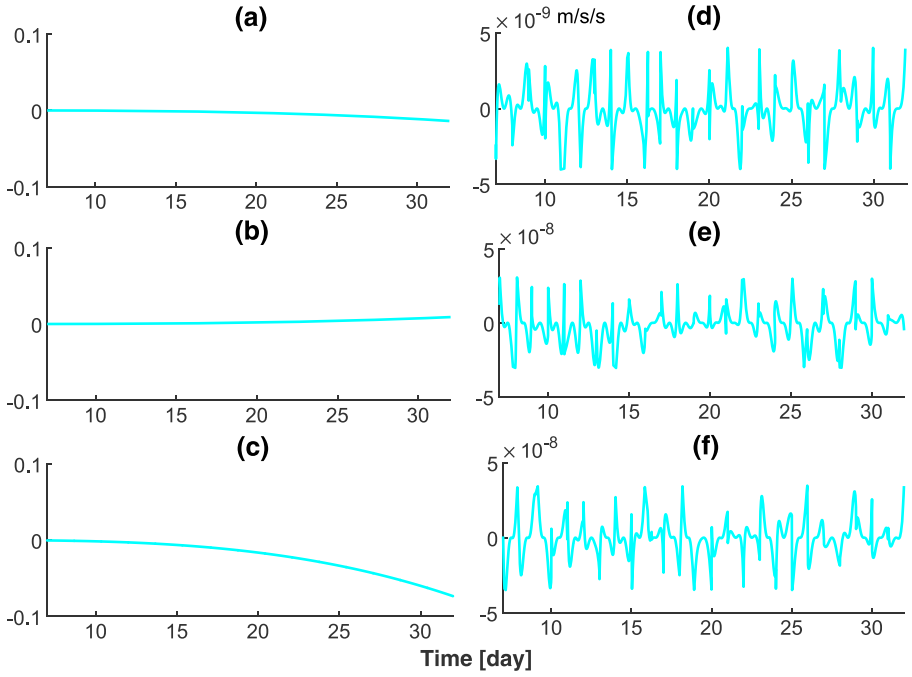

Figure 6. (a–c) Accelerometer scales minus dominant terms (linear and quadratic) in *X*, *Y*, and *Z* axes and (d–f) accelerometer biases minus linear terms in *X*, *Y*, and *Z* directions.

Figure 8 and Table 6 compare the time series of the accelerations in SRF calibrated by case B to those calibrated by other schemes for the month August 2014. Despite some differences of either scale or bias estimates among different methods, both Figure 8 and Table 6 show that the accelerations calibrated on the basis of the schemes G and H are comparable to those calibrated by our method proposed in this paper for all axes, with the standard deviations of no more than7.1×10^{-9} m/s^2. This finding suggests that the accelerometer calibration model based on polynomials is sufficient to calibrate the accelerometer data as other cases. Nevertheless, as confirmed in Table 6, the accelerometer parameters to be solved for each month in the improved method become much less than those in other cases, which contributes more stable normal equation and will be discussed in section 4.3.

4.3. Rationality of the Refined Nongravitational Acceleration Calibration Model

In spite of the difference among various accelerometer calibration models, every calibration model is for deriving better gravity field estimates. It is worthwhile to mention that the excessive parameterization during accelerometer calibration may lead to ill-conditioned or unstable gravity field estimates. Since the nongravitational accelerometer data can be well calibrated by using our polynomial-based method with fewer parameters to be estimated, the normal equation generated by our method is anticipated to be more stable and even leads to an improved gravity field estimate. Hence, in order to verify the rationality of the method proposed in this paper, one indirect way is to compare the condition numbers of the normal equations after

Table 4
Statistics of Accelerometer Parameters With Respect to Monthly and Daily Mean Values

Subtracted term	Accelerometer parameter	Standard deviation
Monthly mean	Bias (***X***| ***Y***| ***Z***)**[m/s/s]**	$\langle 1.2 \times 10^{-9} \mid 8.0 \times 10^{-7} \mid 1.7 \times 10^{-8} \rangle$
	Scale(***X***| ***Y***| ***Z***)	$\langle 1.4 \times 10^{-3} \mid 6.1 \times 10^{-2} \mid 2.4 \times 10^{-2} \rangle$
Daily mean	Bias (*X*| *Y*| *Z*)**/[m/s/s]**	$\langle 1.0 \times 10^{-9} \mid 6.9 \times 10^{-7} \mid 1.4 \times 10^{-8} \rangle$
	Scale(*X*| *Y*| *Z*)	$\langle 1.1 \times 10^{-3} \mid 5.3 \times 10^{-2} \mid 2.0 \times 10^{-2} \rangle$
Linear	Bias (*X*| *Y*| *Z*)**/[m/s/s]**	$\langle 1.1 \times 10^{-9} \mid 1.9 \times 10^{-9} \mid 9.5 \times 10^{-9} \rangle$
Linear and quadratic	Scale(*X*| *Y*| *Z*)	$\langle 3.2 \times 10^{-3} \mid 2.1 \times 10^{-3} \mid 1.7 \times 10^{-2} \rangle$

Table 5
Cases for Gravity Field Modeling

Case	Errors of accelerations and attitudes	Scales		Biases		Parameter amount per month (30 days)
		Period	Polynomial	Period	Polynomial	
B	estimated	One month	3 order	daily	5 order	1,104
G	estimated	One day	0 order	hourly	0 order	4,500
H	estimated	One day	0 order	per 2 hr	1 order	4,500

eliminating the accelerometer parameters and the gravity field model generated by employing our method to those based on other methods. Following this way, one more scheme named case I (solving scales daily and biases hourly without estimating the errors of the accelerometer data and attitude measurements) is designed and then applied to gravity field estimation together with cases B and G, as well as H. Consequently, four gravity field models complete to degree and order 80 based on the GRACE data in August 2014 in terms of geoid degree height relative to EIGEN6C4 are presented in Figure 9. The condition number of the normal equation is 1.19×10^6 for case I, 1.52×10^5 for case B, 6.26×10^5 for case G, and 4.88×10^5 for case H. The condition numbers along with Figure 9 make us draw the conclusions as follows: (a) modeling acceleration and attitude measurement errors can lead to better conditioned normal equation and enhanced gravity field model; (b) estimating accelerometer bias rates in addition to biases is helpful for slightly stabilizing the normal equation and making gravity field estimates better; and (c) the normal equation with the smallest condition number is gathered by using our improved accelerometer calibration model (3-order polynomial for monthly scales and 5-order polynomial for daily biases), which greatly reduces high-frequency noise in the derived gravity field model.

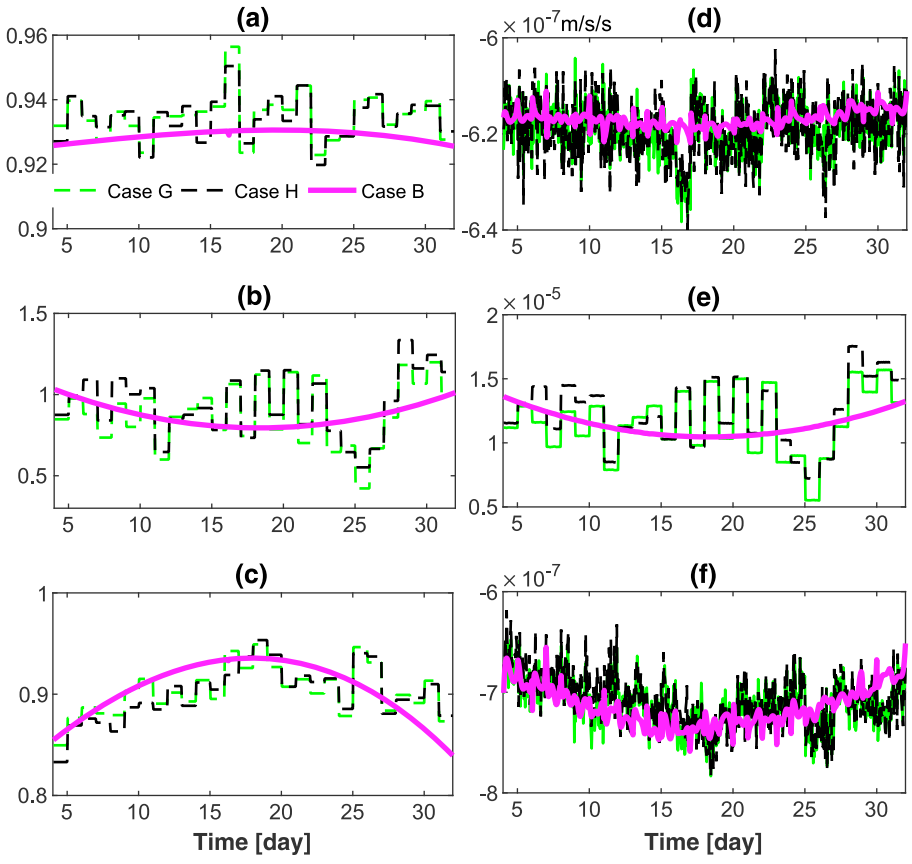

Figure 7. (a–c) Accelerometer scale time series in *X*, *Y*, and *Z* directions and (d–f) accelerometer bias time series in *X*, *Y*, and *Z* axes.

Table 6
Statistics of the Differences Between Our Nongravitational Acceleration Modeling Methods and Others

Case	Calibration	Standard deviation
CaseG versus Case B	Scale $\begin{pmatrix} X \\ Y \\ Z \end{pmatrix}$	$\begin{pmatrix} 6.7\times10^{-3} \\ 1.9\times10^{-1} \\ 2.4\times10^{-2} \end{pmatrix}$
	Bias $\begin{pmatrix} X \\ Y \\ Z \end{pmatrix}$ **[m/s/s]**	$\begin{pmatrix} 4.1\times10^{-9} \\ 2.3\times10^{-6} \\ 1.9\times10^{-8} \end{pmatrix}$
	Acceleration $\begin{pmatrix} X \\ Y \\ Z \end{pmatrix}$ **[m/s/s]**	$\begin{pmatrix} 7.1\times10^{-9} \\ 4.8\times10^{-9} \\ 4.4\times10^{-9} \end{pmatrix}$
Case H versus CaseB	Scale $\begin{pmatrix} X \\ Y \\ Z \end{pmatrix}$	$\begin{pmatrix} 6.7\times10^{-3} \\ 1.8\times10^{-2} \\ 2.3\times10^{-2} \end{pmatrix}$
	Bias $\begin{pmatrix} X \\ Y \\ Z \end{pmatrix}$ **[m/s/s]**	$\begin{pmatrix} 4.3\times10^{-9} \\ 2.4\times10^{-6} \\ 2.0\times10^{-8} \end{pmatrix}$
	Acceleration $\begin{pmatrix} X \\ Y \\ Z \end{pmatrix}$ **[m/s/s]**	$\begin{pmatrix} 7.1\times10^{-9} \\ 4.2\times10^{-9} \\ 3.6\times10^{-9} \end{pmatrix}$

In order to further confirm the improvement contributed by the refined accelerometer data modeling strategies, we combine the yearly normal equations for the period 2003 to 2007 to infer an unconstrained gravity field model up to degree and order 180. The derived model is compared to the gravity field model Tongji-GRACE01 generated on the basis of case I. To keep consistent with the amount of data used in deriving Tongji-GRACE01, the GRACE data that were not included in developing Tongji-GRACE01 (the months from January to June in 2003 and the months containing August, September, and October in 2004) are excluded. The comparison between the resulting model and Tongji-GRACE01 in terms of geoid degree height as shown in Figure 10 exactly demonstrates that the refined acceleration modeling strategies proposed in this paper bring about prominent reduction of high-frequency noise in the gravity field estimates.

4.4. Added Value of Decreased Orbital Altitude and Increased Data Span

The expected lifetime of the GRACE mission before launch is approximately 5 years (https://www.nasa.gov/mission_pages/Grace/overview/index.html), while it successfully offered important scientific information on the Earth's gravity field for about 15 years. It is worthwhile to notice in Figure 11 that the orbital altitudes of both GRACE satellites decreased gradually over the period 2003 to 2011, whereas a dramatic drop occurred in 2012. By July 2016, the orbital altitudes of both satellites were below 370 km. In principle, such a low altitude will become very sensitive to the gravity field signals (especially at high degrees). As one of the refined data processing strategies in this study, using longer time GRACE satellites' data in gravity field modeling as possible as we can is expected to improve the ground track coverage on the medium- and low-latitude regions and eventually may stabilize the gravity field solution.

In addition to the improved ground track coverage, the effect of the remarkably decreased orbital altitudes since 2012 is worth investigating. This is theoretically believed to be a crucial factor for enhancing the gravity field estimation. As indicated in equation (1), the Earth's gravitational potential $V(r,\theta,\lambda)$ is primarily contributed by the term $\left(\frac{a_e}{r}\right)^n (r = a_e + H)$, which means that less attenuation of the gravity field signals (particularly the high-frequency signal) will be caused by a decreased orbital altitude H. To approximately investigate the contribution of the decreased orbital altitude to the gravity field signals, this paper treats the term $\left(\frac{a_e}{r}\right)^n$ as sensitivity of orbital altitude to the gravity field signals. Following this method, the sensitivities of the orbital altitudes to the gravity field signals (for the degrees ranging 2 to 180) since 2004 relative to that in 2003 are plotted in Figure 12. It exactly shows that the decreased orbital altitude benefits increase of sensitivity to the gravity field signals, especially for the high-degree signals. Compared to the orbital altitudes before 2014, the orbital altitudes after 2014 manifest much more significant sensitivity to the high-degree gravity field signals. This means that the utilization of the GRACE data since 2014 is likely to improve the accuracy of the derived gravity field solution.

One method to assess the practical contribution of the decreased orbital altitude is to solve a set of unconstrained gravity field solutions by subtracting the yearly normal equation from the full normal equation for deriving Tongji-Grace02s, which practically reflects the contribution of the yearly GRACE observations. Following this method, the contributions of yearly GRACE data over the period 2003 to 2016 are illustrated in Figure 13a. We can find that the yearly contribution of the GRACE measurements in either 2003 or 2004 is smaller than those in other years, which may be cause by missing observations (beginning and middle of 2003) or repeat ground track (middle to late 2004). For the period spanning 2005 to 2011, the GRACE mission became stable and produced nearly comparable yearly contribution. Nevertheless, the contribution has become pronounced gradually since 2012; especially in the period 2014 to 2016 it went up significantly.

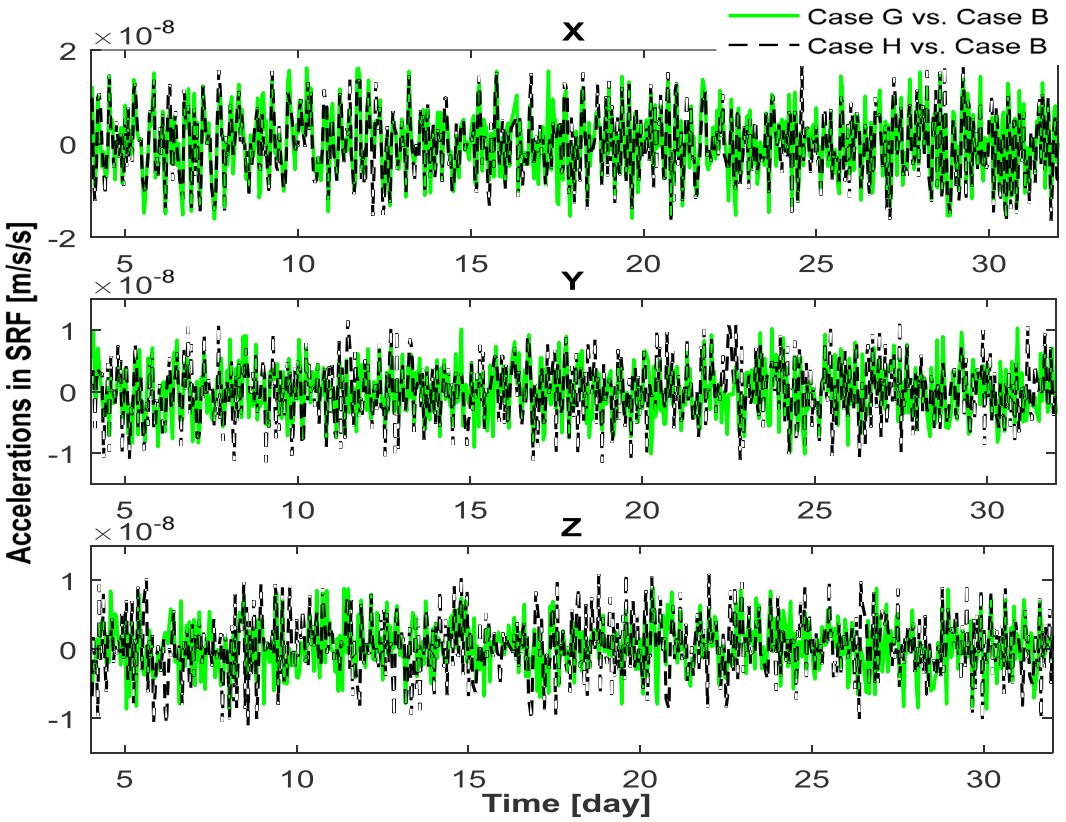

Figure 8. The differences of the calibrated accelerometer data between our nongravitational acceleration modeling approach and others.

As noted above, the thermal control was switched off in 2011 (this means that the quality of the instrument data may be affected since then); hence, the lower orbital altitude is the explanation for the improvements of the gravity field solutions after the thermal control was closed. We also present the condition numbers of the normal equations that are accumulated from the yearly normal equation one by one in Figure 13b. A noticeable drop in condition number for the period spanning 2003 to 2010 can be clearly seen in Figure 13b. This finding demonstrates that only using the observations collected before 2010 is insufficient to well estimate the high-degree static gravity field model. To confirm the above statement, a set of gravity field solutions based on the normal equations accumulated year after year for the period 2005 to 2010 is given in Figure 14a in terms of geoid degree height with respect to EIGEN6C4. With the observations accumulated year after year, the resulting gravity field models tend to become better and better. This finding indeed demonstrates that the increased data span can stabilize the gravity field coefficients at all degrees; thus, we suggest utilizing much longer data span during static gravity field determination.

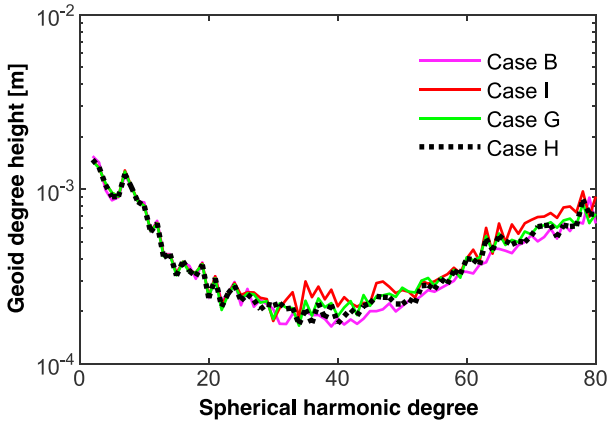

Figure 9. Gravity field solutions in terms of geoid degree height w.r.t EIGEN6C4.

For the period 2011 to 2013, the condition number almost did not change, but it declined remarkably after 2014, which is very worthy to be discussed in detail. Here we further discuss the contributions of the data collected after 2011 to gravity field modeling by matching the condition numbers in Figure 13b to the gravity field solutions after 2011 in Figure 14b. One can see from Figure 13b that the condition numbers of the normal equations slightly decreased year after year over the period 2011 to 2013, which means that the property

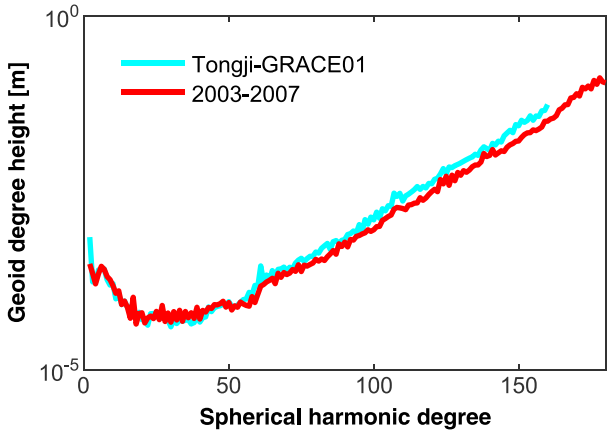

Figure 10. Gravity field solution based on the same data span as Tongji-GRACE01.

of the accumulated normal equation during this period did not significantly change. Nevertheless, the condition number of the accumulated normal equation became dramatically smaller after 2014, because the GRACE orbital altitudes dropped down significantly in this time period, which eventually led to the pronounced enhancements on gravity field modeling as illustrated in Figure 14b. It also suggests that the significantly lower orbital altitudes are very sensitive to the gravity field signals at high degrees.

5. Error Analyses of Tongji-Grace02s and Tongji-Grace02k With Respect to EIGEN6C4

To assess the errors of both Tongji-Grace02s and Tongji-Grace02k models, the latest GRACE-only models (including GGM05S, AIUB-GRACE03S, Tongji-GRACE01, ITU_GRACE16, HUST-Grace2016s, ITSG-Grace2014s, and ITSG-Grace2014k) developed by different data processing centers are used for comparison. Both ITSG-Grace2014s and ITSG-Grace2014k are complete to degree and order 200, which were obtained by Graz University of Technology on the basis of the dynamic approach (Mayer-Gürr et al., 2014). Using the dynamic approach, GGM05S up to degree and order 180 and HUST-Grace2016s with a maximum degree and order of 160 were generated by Center for Space Research (CSR) and Huazhong University of Science and Technology respectively. Tongji-GRACE01 with a maximum degree and order of 160 is the first release of Tongji static gravity field solution series derived by Tongji University via the modified short-arc approach. Bern University determined the AIUB-GRACE03S model complete to degree and order 180 by applying the celestial mechanics method (Jäggi et al., 2010). Based on an improved energy balance approach (Shang et al., 2015), the ITU_GRACE16 model complete to degree and order 180 was calculated by The Ohio State University.

5.1. Geoid Degree Height Comparison

To comprehensively discuss the spectrums of the estimated geopotential coefficients, we compare the geoid degree heights of both Tongji-Grace02s and Tongji-Grace02k with respect to EIGEN6C4 to those of GGM05S, AIUB-GRACE03S, Tongji-GRACE01, ITU_GRACE16, HUST-Grace2016s, ITSG-Grace2014s, and ITSG-Grace2014k in Figure 15a. We can conclude from Figure 15a that (1) for the low degrees, the discrepancies among various models are quite obvious, which is mainly attributed to the remaining unmodeled time-variable signals and varying reference epochs used in the models; (2) ITU_GRACE16 shows the largest errors for the coefficients above degree 60; (3) less difference at high degrees (beyond degree 60) can be found among AIUB-

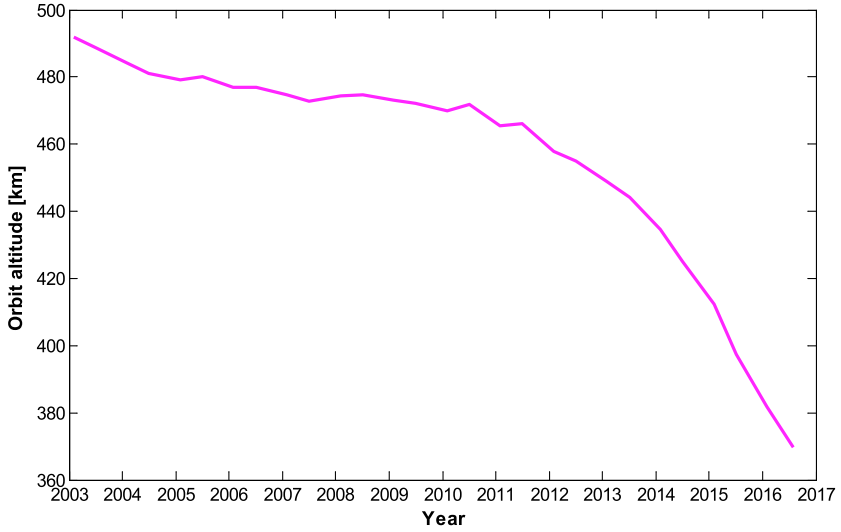

Figure 11. Orbital altitudes of the GRACE satellites.

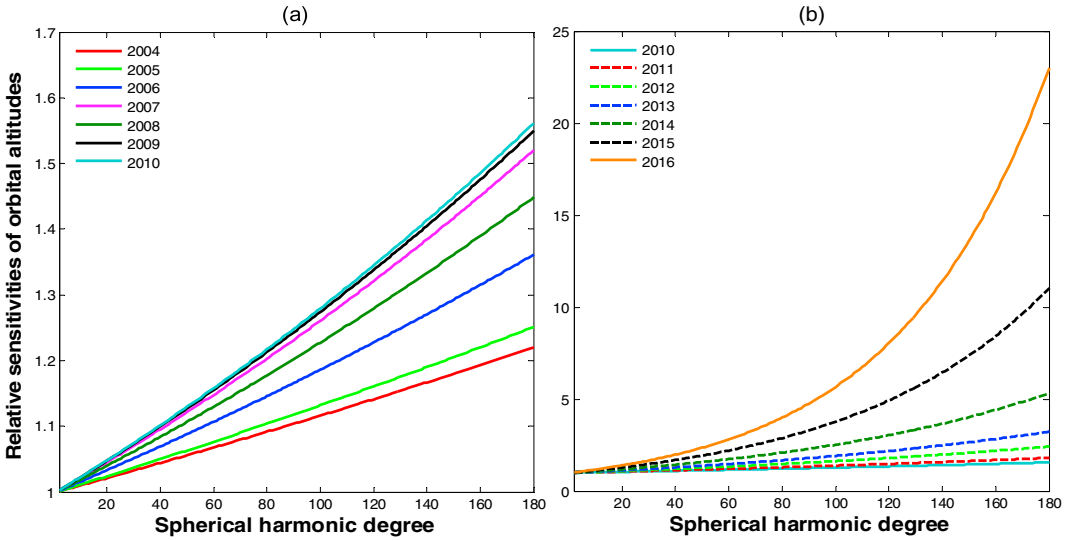

Figure 12. Relative sensitivities of orbital altitudes to the Earth's gravitational potential.

GRACE03S, Tongji-GRACE01, and HUST-Grace2016s, demonstrating that these models at the high degrees are comparable; (4) Tongji-Grace02s and Tongji-Grace02k show good agreement with ITSG-Grace2014s and ITSG-Grace2014k for the degrees ranging 60 to 140; (5) although both ITSG-Grace2014s and ITSG-Grace2014k are remarkably better than GGM05S, AIUB-GRACE03S, Tongji-GRACE01, ITU_GRACE16, and HUST-Grace2016s at the high degrees, they manifest much more errors for the degrees above 140 compared with either Tongji-Grace02s or Tongji-Grace02k, and even the regularized solution ITSG-Grace2014k does not perform better than the unconstrained model Tongji-Grace02s; and (6) the errors of the regularized static gravity field solutions ITSG-Grace2014k and Tongji-Grace02k at the high degrees are distinctly reduced compared to those of the corresponding unconstrained models; moreover, Tongji-Grace02k has the least error for the degrees beyond 140 among all the GRACE-only models, suggesting that the regularization method based on the Kaula rule and the determined regularization factor are capable of significantly reducing the errors of the solved gravity field models. For further comparisons, the formal errors of these models are presented in Figure 15b. It clearly demonstrates that (1) GGM05S and ITU-GRACE16 have relatively larger formal errors; (2)

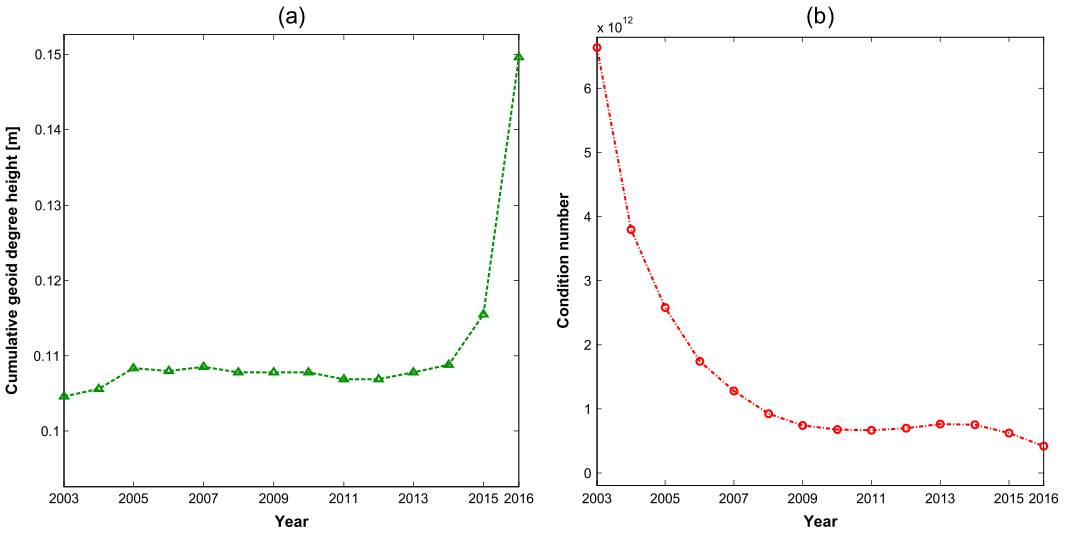

Figure 13. (a) Time series of contributions of yearly GRACE observations in terms of cumulative geoid degree height w.r.t EIGEN6C4; (b) time series of condition numbers of normal equations generated from increased data span.

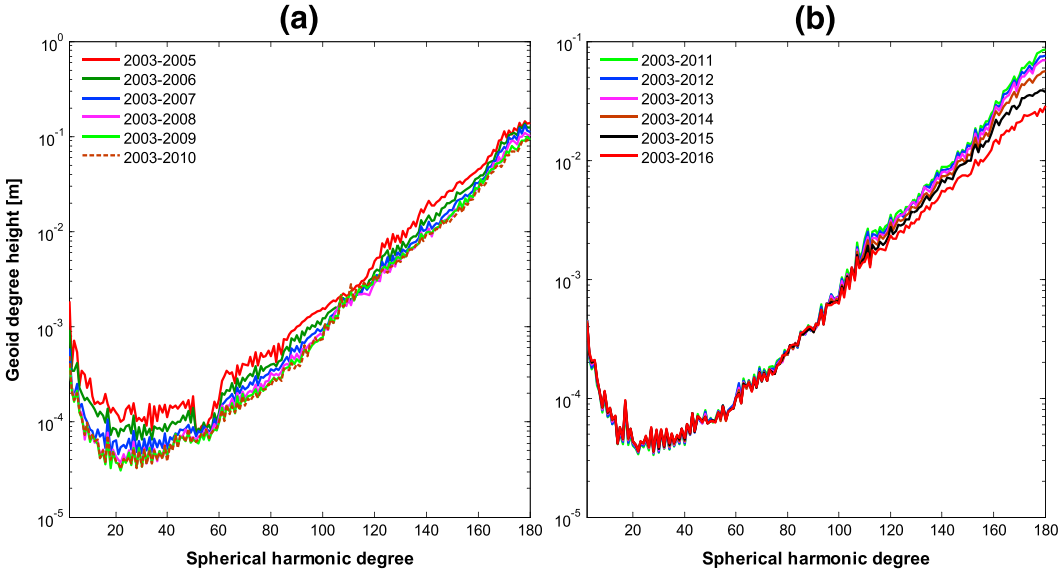

Figure 14. Geoid degree heights of gravity field solutions generated from increased data span w.r.t EIGEN6C4.

Tongji-Grace02s and Tongji-Grace02k achieve much less formal errors among all the models; (3) for other models, the formal errors are generally at the same level; and (4) the formal errors are reduced via regularization to some extent.

5.2. Gravity Anomaly Comparison

With an attempt to investigate the spatial distributions of the errors of various GRACE-only models, we further compute global gravity anomaly discrepancies of the models (i.e., GGM05S, ITU_GRACE16, ITSG-Grace2014s, ITSG-Grace2014k, Tongji-Grace02s, and Tongji-Grace02k) with respect to EIGEN6C4 truncated to degree and order 180. The models (namely, AIUB-GRACE03S, Tongji-GRACE01, and HUST-Grace2016s) only complete to degree and order 160 are not selected for comparisons since this section concentrates on the high-degree errors. The global gravity anomaly discrepancies illustrated in Figure 15 clearly show that both GGM05S and ITU_GRACE16 are severely contaminated by errors, though GGM05S seems a little better than

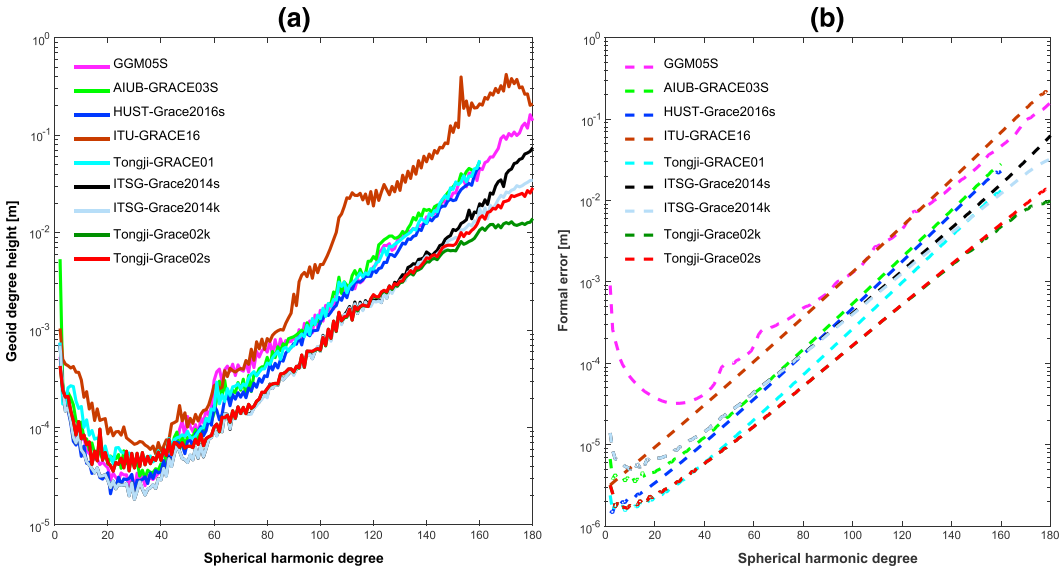

Figure 15. (a) Geoid degree heights of GRACE-only models w.r.t. EIGEN6C4 and (b) formal errors of GRACE-only models.

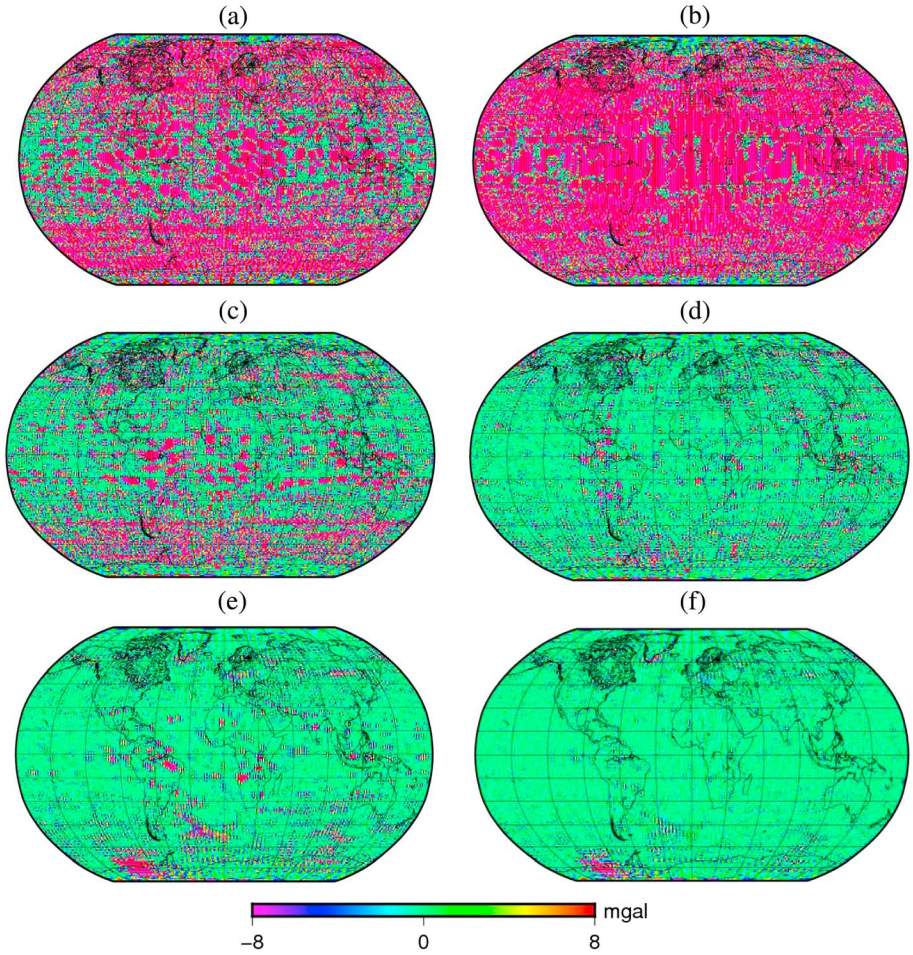

Figure 16. Gravity anomalies of different GRACE-only models w.r.t. EIGEN6C4: (a) GGM05S, (b) ITU_GRACE16, (c) ITSG-Grace2014s, (d) ITSG-Grace2014k, (e) Tongji-Grace02s, and (f) Tongji-Grace02k.

ITU_GRACE16 on the medium- and low-latitude regions. Although the errors of ITSG-GRACE2014s are still obvious over oceans and lands (especially in the southern hemisphere), the errors of ITSG-Grace2014s are much less than those of GGM05S and ITU_GRACE16 models. Nevertheless, the errors of Tongji-Grace02s are considerably reduced (especially over oceans) among the unconstrained modes and the regularized solutions (both ITSG-Grace2014k and Tongji-Grace02k) greatly suppress the errors in comparison to the corresponding unconstrained ones. Compared to Tongji-Grace02k, however, the errors of ITSG-Grace2014k are evident, particularly on the medium- and low-latitude regions (this is probably attributed to the uneven altitude distribution between northern and southern hemispheres of GRACE). For further analyses, the mean standard deviations of the global gravity anomaly differences are calculated, which are 22.9, 37.9, 6.8, 4.2, 4.3, and 3.0 mgals for GGM05S, ITU_GRACE16, ITSG-Grace2014s, ITSG-Grace2014k, Tongji-Grace02s, and Tongji-Grace02k, respectively, confirming the superior quality of both Tongji-Grace02s and Tongji-Grace02k. However, both Tongji-Grace02s and Tongji-Grace02k present more significant variations in the Antarctica compared to ITSG-Grace2014k, which is practically caused by different reference epochs used in these models. As noted in section 3.3, the reference epoch for our models is 1 January 2005, while both ITSG-Grace2014s and ITSG-Grace2014k use the reference epoch of 1 January 2008.

The gravity anomalies of the GRACE-only models with respect to EIGEN6C4 truncated to degree and order of 180 over the Indian Ocean, the North Atlantic, and the global oceans are anticipated to be small, since the oceanic tidal and nontidal effects have been mostly removed by the force models during gravity field determination. Hence, the gravity anomaly discrepancies are approximately treated as the errors of the GRACE-only models in this study. The mean standard deviations in Table 7 clearly demonstrate that the smallest

Table 7
Mean Standard Deviation Values (in Unit of mgal) of the Gravity Anomaly Differences Over Oceans

Region	GGM 05S	ITU-GRACE 16	ITSG-grace 2014s	ITSG-grace 2014 k	Tongji-grace 02 s	Tongji-grace 02 k	Improved rate of Tongji-Grace02s	Improved rate of Tongji-Grace02k
Indian Ocean	14.3	24.1	8.9	3.9	4.3	2.6	107%	50%
North Atlantic	19.0	37.3	5.3	3.6	2.8	2.0	89%	80%
Global oceans	24.6	32.2	6.6	3.8	3.7	2.5	99%	48%

error is achieved by Tongji-Grace02s among the unconstrained GRACE-only models. Compared to ITSG-Grace2014s, the error reductions of Tongji-Grace02s over the Indian Ocean, the North Atlantic, and the global oceans are about 107%, 89%, and 99% separately. For the regularized GRACE-only models, both ITSG-Grace2014k and Tongji-Grace02k can suppress the errors to a great extent, whereas Tongji-Grace02k is still better than ITSG-Grace2014k, with the improvements of 50%, 80%, and 48% relative to ITSG-Grace2014k for the cases over the Indian Ocean, the North Atlantic, and the global oceans, respectively. Over the Indian Ocean, the error distributions of the GRACE-only models in terms of gravity anomalies are further presented in Figure 17. As anticipated, the spatial errors of Tongji-Grace02s have been significantly suppressed in comparison with those of the other unconstrained models. Among the six GRACE-only models, ITU_GRACE16 has the most spatial errors and Tongji-Grace02k is contaminated by the smallest spatial error. However, both Table 7 and Figure 17 prove that GRACE mission alone is insufficient for estimating marine gravity field because of the dominant spatial errors contained in the solutions.

6. Quality Assessments of Tongji-Grace02s and Tongji-Grace02k

In this section we evaluate the quality of various GRACE-only models on the basis of independent data sources, namely, the GNSS/Leveling data and DTU13 oceanic gravity measurements.

6.1. Assessment by Using DTU13 Oceanic Gravity Product

To assess the GRACE models, an independent data source, the DTU13 product (Andersen et al., 2014) with a spatial resolution of $2' \times 2'$ derived from altimetry measurements of multisatellites by Technical University of Denmark, is applied. In this section, we compare the DTU13 oceanic gravity data over the Centric Atlantic

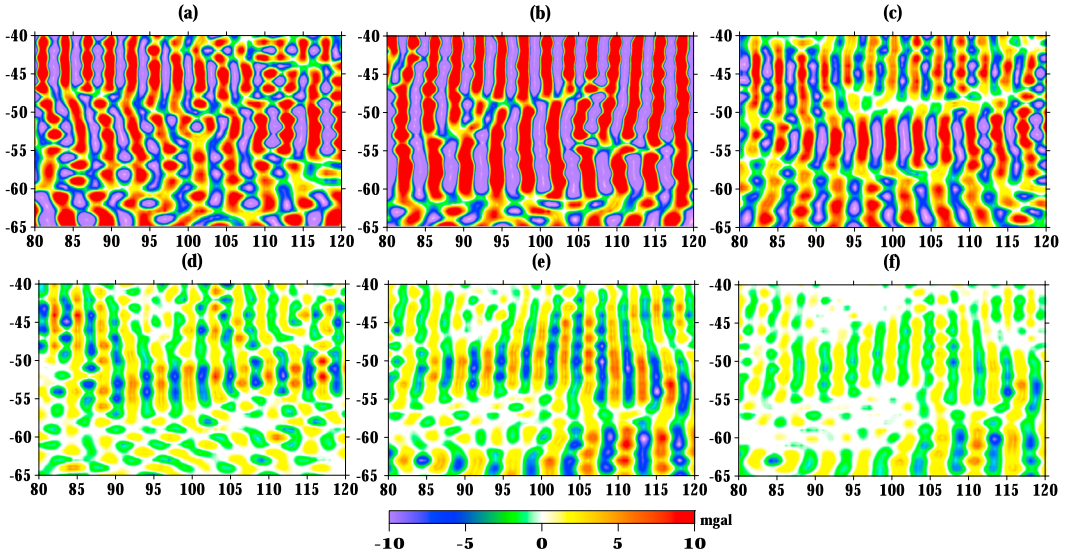

Figure 17. Gravity anomalies of different GRACE-only models w.r.t. EIGEN6C4 over the Indian Ocean: (a) GGM05S, (b) ITU_GRACE16, (c) ITSG-Grace2014s, (d) ITSG-Grace2014k, (e) Tongji-Grace02s, and (f) Tongji-Grace02k.

Table 8
Mean Standard Deviation Values of the Differences (in Unit of mgal) Between the DTU13 Data and the Gravity Anomalies Computed From the Models Over the Centric Atlantic (Case A) and the North Pacific (Case B) (Indicates Unavailable Test)*

Case	Degree	GGM 05S	ITU-GRACE 16	AIUB-GRACE 03S	Tongji-GRACE 01	HUST-Grace 2016s	ITSG-Grace 2014s	ITSG-Grace 2014 k	Tongji-Grace 02 s	Tongji-Grace 02 k
A	60	0.81	0.81	0.81	0.81	0.81	0.81	0.81	0.81	0.81
	90	0.81	0.81	0.81	0.81	0.81	0.81	0.81	0.81	0.81
	120	0.81	1.28	0.82	0.85	0.85	0.81	0.81	0.82	0.82
	160	3.94	34.74	3.51	3.74	3.27	2.31	1.41	2.31	1.39
	180	10.52	72.80	*	*	*	6.79	4.06	4.18	2.42
B	60	2.25	2.25	2.25	2.25	2.25	2.25	2.25	2.25	2.25
	90	2.25	2.25	2.25	2.25	2.25	2.25	2.25	2.25	2.25
	120	2.25	2.29	2.28	2.27	2.25	2.25	2.25	2.26	2.26
	160	3.17	10.62	4.84	4.09	3.29	2.60	2.57	1.47	2.30
	180	10.74	15.07	*	*	*	4.83	4.44	3.05	2.61

([26°N, 36°N], [255°E, 265°E]) and the North Pacific ([30°N, 40°N], [165°E, 175°E]) with those computed from the GRACE-only models (i.e., GGM05S, ITU_GRACE16, AIUB-GRACE03S, Tongji-GRACE01, HUST-Grace2016s, ITSG-Grace2014s, ITSG-Grace2014k, Tongji-Grace02s, and Tongji-Grace02k) truncated to different degrees (i.e., 60, 90, 120, 160, and 180). In order to avoid spectrum omission, the geopotential coefficients beyond the truncated degrees are replaced with those of the EIGEN6C4 up to degree and order 2190 in computing the gravity anomalies. This is reasonable since the resolutions of the GRACE-only models are limited to a certain degree and what we mostly concern about in this study is the gravity field signals at the medium and long waves, which are greatly contributed by the GRACE mission. In view of that the spatial resolution of EIGEN6C4 is approximately $5' \times 5'$, which does not match the spatial resolution of the DTU13 product, the DTU13 data are needed to compress into $5' \times 5'$. Here we give out the gravity anomaly differences between DTU13 and the GRACE-only models in Table 8.

One can see from Table 8 that for the cases truncated to degrees 60, 90, and 120 over both oceans, all the unconstrained and regularized models have the similar mean standard deviations, which are probably caused by the difference between DTU13 data and EIGEN6C4, indicating that the quality of the lower degree coefficients of different models cannot be identified by DTU13 data. However, the differences become much pronounced when truncated to degree either 160 or 180. This finding suggests that (1) the GRACE mission show much stronger sensitivity to the geopotential coefficients below degree 120 and (2) the higher degree coefficients from GRACE are greatly contaminated by errors, which directly reflect the quality of the GRACE-only models. For the case truncated to degrees 160, ITU_GRACE16 has the largest difference (with 34.74 and 10.62 mgals in the Centric Atlantic and the North Pacific, respectively), but Tongji-Grace02s shows the best agreement to the DTU13 data (with 2.31 and 1.47 mgals over the Centric Atlantic and the North Pacific separately) among all the unconstrained models. Furthermore, Tongji-Grace02s still shows the best agreement to the DTU13 data among all the unconstrained models when the coefficients up to degree and order 180 are used (with 4.18 and 3.05 mgals in the Centric Atlantic and the North Pacific, respectively, corresponding to 62% of enhancement over the Centric Atlantic and 58% of improvement over the North Pacific relative to ITSG-Grace2014s). During truncation to either 160 or 180, the regularized solutionITSG-Grace2014k remains more prominent errors than Tongji-Grace02k (with 2.42 and 2.61 mgals in the Centric Atlantic and the North Pacific respectively, corresponding to the error reductions of about 68% and 70% relative to ITSG-Grace2014k in the Centric Atlantic and the North Pacific, respectively) in spite of ITSG-Grace2014k showing much better accuracy in comparison to ITSG-Grace2014s.

Table 8 just reflects the overall noise levels of the GRACE-only models. We further show the spatial error distributions of the GRACE-only models (GGM05S, ITU_GRACE16, ITSG-Grace2014s, ITSG-Grace2014k, Tongji-Grace02s, and Tongji-Grace02k) over the North Pacific in terms of gravity anomalies relative to DTU13 data in Figure 18 to get more insights into the quality of the GRACE-only models. The patterns of the gravity anomaly differences depicted in Figure 18 allow us to draw the following conclusions: (1) both GGM05S and ITU_GRACE16 are severely contaminated by the spatial errors, while Tongji-Grace02s contains the least error among all the unconstrained models, and (2) ITSG-Grace2014s and ITSG-Grace2014k (especially the regularized solution ITSG-Grace2014k) show better performance when comparing with GGM05S and ITU_GRACE16,

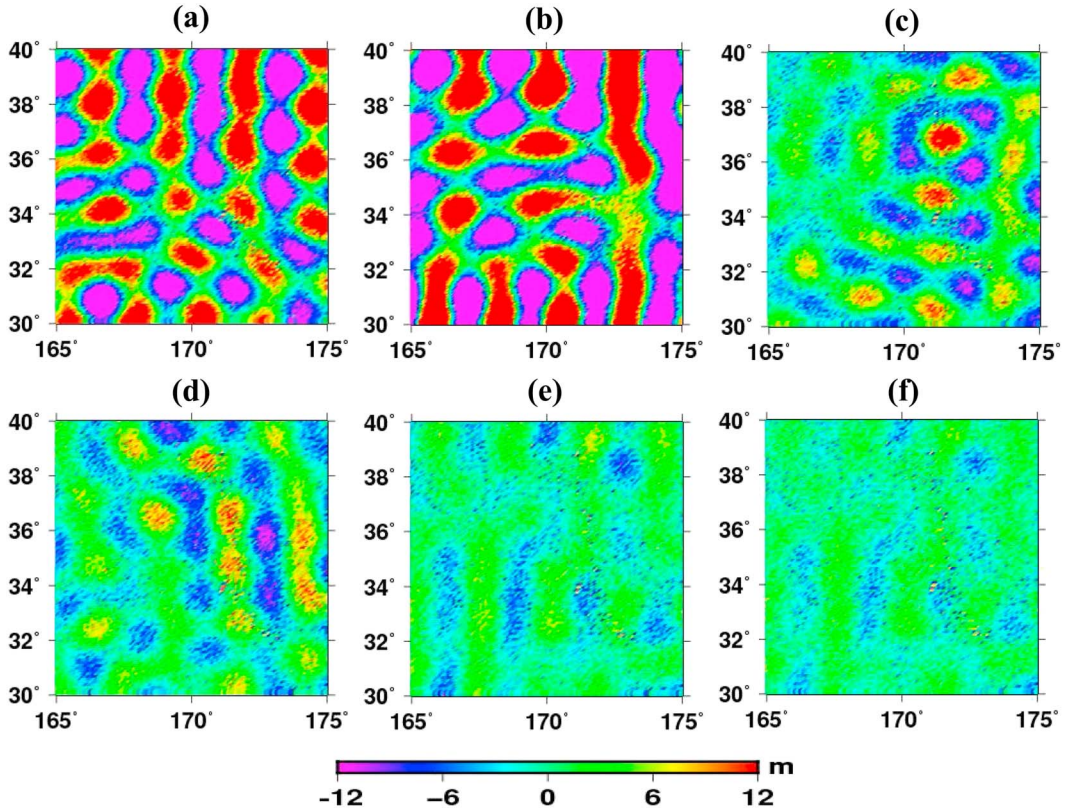

Figure 18. Gravity anomaly differences between the DTU13 gravity data and the GRACE-only models over the North Pacific: (a) GGM05S, (b) ITU_GRACE16, (c) ITSG-Grace2014s, (d) ITSG-Grace2014k, (e) Tongji-Grace02s, and (f) Tongji-Grace02k.

but they are worse than Tongji-Grace02k. It is not necessary to depict the patterns in the Centric Atlantic as they do not change the above conclusions.

6.2. Evaluated by GNSS/Leveling Data

As another independent data source, GNSS/Leveling observations are usually employed for evaluating static gravity field models. One of the services included in the International Center for Global Earth Models (ICGEM; Barthelmes & Köhler, 2016) is to validate the gravity field solutions available on the ICGEM based on the GNSS/Leveling data. The GRACE-only models analyzed above except for Tongji-Grace02k (will be submitted to the ICGEM shortly) are available on the ICGEM, which were assessed by the ICGEM on the basis of the GNSS/Leveling observations over the USA, Canada, Europe, Japan, Australia, and Brazil. The mean standard deviation values derived from the differences between the GNSS/Leveling data and the geoid heights from the latest GRACE-only models are given in Figure 19. Though the spectrum omissions beyond the maximum degrees of the GRACE-only models during computation were not considered in the ICGEM service, some conclusions still can be drawn from Figure 19 when comparing the models with the same spatial resolution. In Figure 19, Tongji-Grace02s is significantly better than GGM05S and ITU_GRACE16 for all the tests, which improves 57% and 446% of accuracies in the overall GNSS/Leveling data test relative to GGM05S and ITU_GRACE16, respectively. Additionally, the comparisons between the unconstrained solution ITSG-Grace2014s and the regularized model ITSG-Grace2014k for all the tests prove that the regularization method can suppress the errors of the gravity field models.

For more comprehensive comparisons, further analyses are carried out by using the GNSS/Leveling data sets in both the Canada and Mexico. When computing the geoid heights on the basis of the GRACE-only models (i.e., GGM05S, ITU_GRACE16, AIUB-GRACE03S, Tongji-GRACE01, HUST-Grace2016s, ITSG-Grace2014s, ITSG-Grace2014k, and Tongji-Grace02s and Tongji-Grace02k), they are truncated to particular degrees (i.e., 60, 90, 120, 160, and 180) and the coefficients at higher degrees are replaced with those of EIGEN6C4. As

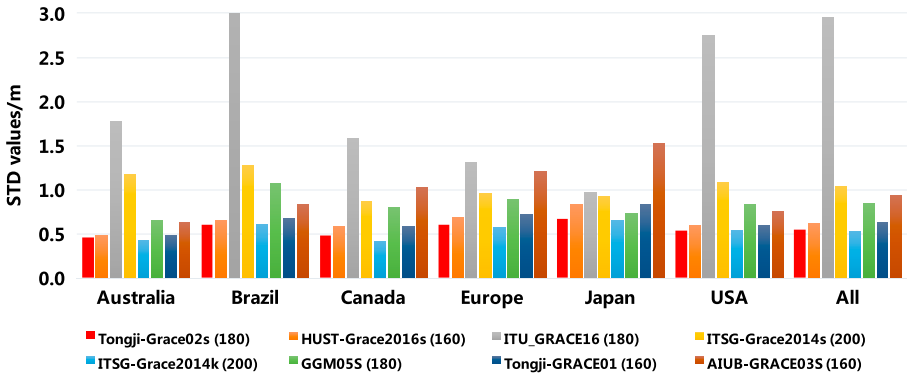

Figure 19. Mean standard deviation values (in unit of cm) of the differences between the GNSS/Leveling data and the geoid heights computed from the GRACE-only models (calculated values from the ICGEM).

shown in Table 9, the mean standard deviations of the differences between the GNSS/Leveling data and the computed geoid heights lead to the comparable conclusions as the validations based on the DTU13 oceanic gravity data. Although the discrepancies are not obvious for the cases below 120, Tongji-Grace02s has the best quality among all the unconstrained solutions and Tongji-Grace02k shows the best performance among all the models when truncated to degree either 160 or 180. Especially for the case truncated to degree 180, Tongji-Grace02k obtains 9% and 6% of enhancements in comparison to ITSG-Grace2014k over the tests of the Canada and Mexico separately. Even better, using the same truncation, 13% and 23% of improvements with respect to ITSG-Grace2014s are achieved by Tongji-Grace02s during the verifications over the Canada and Mexico, respectively. We also plot the spatial distributions of the geoid height differences between the GNSS/Leveling data and the six models in the Mexico when truncated to degree 180 in Figure 20. The spatial error distributions of both GGM05S and ITU_GRACE16 are more pronounced than those of the others. Overall, the regularized solution Tongji-Grace02k shows a good agreement with ITSG-Grace2014kin terms of spatial error pattern in the Mexico, and the same conclusion can be conducted when comparing the unconstrained solution Tongji-Grace02s to ITSG-Grace2014s.

7. Concluding Remarks

The successful GRACE mission measured the Earth's gravity field for almost 15 years, offering a long time series of observations to scientists for developing the Earth's gravity fields. On behalf of improving the accuracy of high-degree static GRACE-only gravity field models, some updated data processing strategies have been presented in this paper. In general, the main efforts can be summarized as follows: (1) adopting the methodology that models the errors of the acceleration and attitude observations to reduce the high-frequency noise, (2) refining the method to calibrate the accelerometer measurements by using a 3-order polynomial for the monthly accelerometer scales and a 5-order polynomial for the daily accelerometer biases, (3) using the currently longest time series of GRACE data (January 2003 to July 2016) to compute unconstrained static gravity field model, and (4) further stabilizing the normal equation by applying the regularization method based on the Kaula rule and the regularization factor determined by minimizing the trace of MSE.

During the discussions on the refined data processing strategies, we find that (1) modeling the acceleration and attitude data errors is beneficial for decreasing the errors of the derived gravity field model at the high degrees; (2) the improved accelerometer calibration method has the comparable ability to calibrate the non-gravitational accelerations as other methods, while it reduces almost triple amount of parameters to be solved and consequently achieves better conditioned normal equation and noticeable improvement in gravity field determination; (3) estimating the acceleration and attitude data errors also can suppress high-frequency noise in the solved gravity field solution; (4) longer GRACE data span is demonstrated to be crucial for improving geopotential coefficients at all degrees before the system of the normal equation becomes stable (mainly before 2010), while less improvement can be contributed by further increased GRACE data span (e.g., from 2011 to 2013) once it becomes stable; and (5) the GRACE data with remarkably lower orbital altitudes over the period 2014 to 2016 can greatly reduce the condition number of the normal equation and

Table 9
Mean Standard Deviation Values of the Differences (in Unit of cm) Between the GNSS/Leveling Data in the Canada and the Geoid Heights Computed From the GRACE-Only Models

Case	Degree	GGM 05S	ITU-Grace 16	AIUB-Grace 03S	Tongji-Grace 01	HUST-Grace 2016s	ITSG-Grace 2014s	ITSG-Grace 2014 k	Tongji-Grace 02 s	Tongji-Grace 02 k
Canada	60	24.6	24.5	24.5	24.6	24.5	24.5	24.5	24.6	24.6
	90	24.5	24.5	24.5	24.6	24.6	24.6	24.5	24.6	24.6
	120	24.6	25.0	24.4	24.8	24.5	24.5	24.5	24.5	24.5
	160	26.7	40.6	25.1	28.9	29.5	25.5	25.2	24.5	24.4
	180	50.6	223.4	*	*	*	29.4	27.7	26.1	25.4
Mexico	60	26.2	26.2	26.2	26.2	26.2	26.2	26.2	2.62	26.2
	90	26.2	26.2	26.2	26.2	26.2	26.2	26.2	26.2	26.2
	120	26.2	27.0	26.3	26.3	26.2	26.2	26.2	26.2	26.2
	160	29.3	47.5	30.9	30.4	28.0	26.5	26.4	26.5	26.4
	180	58.8	202.7	*	*	36.7	34.6	27.4	28.2	26.5

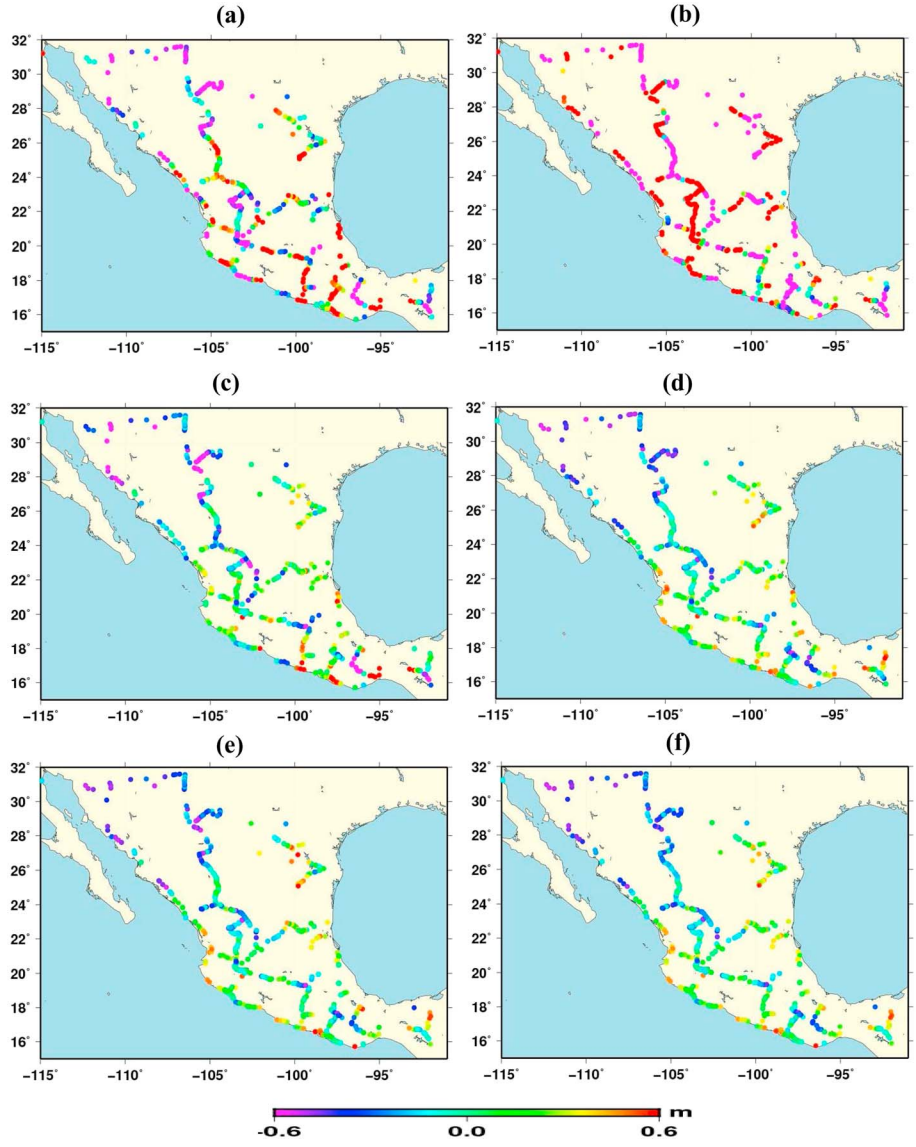

Figure 20. Geoid height differences between the GNSS/Leveling data and the GRACE-only models in the Mexico: (a) GGM05S, (b) ITU_GRACE16, (c) ITSG-Grace2014s, (d) ITSG-Grace2014k, (e) Tongji-Grace02s, and (f) Tongji-Grace02k.

result in significantly improved gravity field model, which is because the lower orbital altitude shows much stronger sensitivity to the high-frequency signals in gravity field.

Based on the refined data processing strategies above, an unconstrained static GRACE-only gravity field solution called Tongji-Grace02s up to degree and order 180 is successfully inferred and a regularized static model named Tongji-Grace02k with the same degree is derived by applying the Kaula rule to the normal equation for the degrees ranging from 81 to 180. Both Tongji-Grace02s and Tongji-Grace02k are compared to the latest GRACE-only models (i.e., GGM05S, AIUB-GRACE03S, Tongji-GRACE01, ITU_GRACE16, HUST-Grace2016s, ITSG-Grace2014s, and ITSG-Grace2014k) and verified by both GNSS/Leveling data and DTU13 oceanic gravity data. The concluding remarks from the comparisons and validations are as follows:

1. The geoid degree heights with respect to EIGEN6C4 demonstrate that Tongji-Grace02s has the least error among all the unconstrained models and Tongji-Grace02k performs the best (particularly for the degrees above 140) among all the models.
2. Both Tongji-Grace02s and Tongji-Grace02k are compared to other GRACE-only models in terms of gravity anomalies relative to EIGEN6C4 over the globe, the global oceans, the Indian Ocean, and the North Atlantic. The comparisons show that much less spatial error occurs in Tongji-Grace02s among all the unconstrained models and the best performance is achieved by Tongji-Grace02k among all the models. The mean standard deviations for the gravity anomalies are 22.9, 37.9, 6.8, 4.2, 4.3, and 3.0 mgals for GGM05S, ITU_GRACE16, ITSG-Grace2014s, ITSG-Grace2014k, Tongji-Grace02s, and Tongji-Grace02k, respectively. For the testes over the global oceans, the Indian Ocean and the North Atlantic, Tongji-Grace02s reduces no less than 89% of noise relative to ITSG-Grace2014s, and Tongji-Grace02k achieves at least 48% of noise reduction relative to ITSG-Grace2014k.
3. The assessments using both the DTU13 oceanic gravity data over two oceans (i.e., the Centric Atlantic and the North Pacific) and the GNSS/Leveling data over two lands areas (i.e., the Mexico and the Canada) support that the unconstrained solution Tongji-Grace02s and the regularized model Tongji-Grace02k show good agreements with other models (GGM05S, ITU_GRACE16, ITSG-Grace2014s, and ITSG-Grace2014k) for the degrees below 120. Nevertheless, the best agreement to DTU13 data is reached by Tongji-Grace02s among all the unconstrained models and the most satisfactory performance belongs to Tongji-Grace02k among all the models for the degrees beyond 120.
4. The mean standard deviations of the gravity anomalies from Tongji-Grace02sup to degree and order 180 relative to DTU13 data are 4.18 and 3.05 mgals in the Centric Atlantic and the North Pacific, respectively (indicating 62% and 58% of improvements over the Centric Atlantic and the North Pacific separately compared to those from ITSG-Grace2014s). For the regularized solutions (i.e., Tongji-Grace02k and ITSG-Grace2014k), 68% and 70% of improvements over the Centric Atlantic and the North Pacific respectively are gained by Tongji-Grace02k compared to ITSG-Grace2014k. Furthermore, Tongji-Grace02k achieves 9% and 6% of improvements compared to ITSG-Grace2014k in the GNSS/Leveling tests over the Canada and Mexico separately. Moreover, Tongji-Grace02s has 13% and 23% of improvements with respect to ITSG-Grace2014s in the same tests over the Canada and Mexico, respectively.

Acknowledgments

This work is mainly supported by the National Natural Science Foundation of China (41474017, 41731069, and 41674006). It is also partly sponsored by the State Key Laboratory of Geo-information Engineering (SKLGIE2014-M-1-2), the Strategic Priority Research Program of the Chinese Academy of Sciences (XDB23030100), and the Program of Application and Demonstration System of High Resolution Remote Sensing in Surveying and Mapping. The Fundamental Research Funds for the Central University (18CX02066A) also should be acknowledged for its support. The GRACE Level-1B data provided by JPL can be downloaded from JPL ftp (podaac. Jpl. nasa.gov), and the kinematic orbit measurements offered by Graz University of Technology can be accessed via ftp://ftp.tugraz.at/outgoing/ITSG/tvgogo/orbits/GRACE/. The static models used for comparison are available at the ICGEM (http://icgem.gfz-potsdam.de/ICGEM/). The GNSS/Leveling data can be downloaded from http://www.ngs.noaa.gov/GEOID/GEOID12, and the DTU13 data from Technical University of Denmark can be found at https://ftp.space.dtu.dk/pub/DTU13/. Prof. John Ries from the Center for Space Research should be acknowledged for his help on comparing solid Earth tides. We are also very grateful to the Editors, Prof. Paul Tregoning, and two anonymous reviewers for their valuable comments, which significantly improve the quality of our original manuscript.

References

Andersen, O. B., Knudsen, P., Kenyon, S., & Holmes, S. (2014, June). *Global and Arctic marine gravity field from recent satellite altimetry (DTU13)*. The 76th EAGE Conference and Exhibition, Amsterdam, Netherlands. https://doi.org/10.3997/2214-4609.20140897

Bandikova, T., & Flury, J. (2014). Improvement of the GRACE star camera data based on the revision of the combination method. *Advances in Space Research*, *54*(9), 1818–1827. https://doi.org/10.1016/j.asr.2014.07.004

Bandikova, T., Meyer, U., Klinger, B., Tregoning, P., Flury, J., & Mayer-Gürr, T. (2014, September). *Improved star camera attitude data and their effect on the gravity field*. GRACE Science Team Meeting, Potsdam, Germany.

Barthelmes, F., & Köhler, W. (2016). International Centre for Global Earth Models (ICGEM). In H. Drewes, F. Kuglitsch, J. Adám, & S. Rózsa (Eds.), The geodesists handbook 2016. *Journal of Geodesy*, *90* (10), 907–1205. https://doi.org/10.1007/s00190-016-0948-z

Behzadpour, S., Mayer-Gürr, T., & Flury, J. (2016, April). *Robust estimation of error covariance functions in GRACE gravity field determination*. EGU General Assembly Conference (Vol. 18, p. 11,567), Vienna, Austria. https://doi.org/10.13140/RG.2.1.4128.0246

Bender, P. L., Wiese, D. N., & Nerem, R. S. (2008). A possible dual-GRACE mission with 90 degree and 63 degree inclination orbits. *Proceedings of the Third International Symposium on Formation Flying, Missions and Technologies* (pp. 1–6). Noordwijk, Netherlands: ESA/ESTEC.

Bettadpur, S. (2009). Recommendation for a-priori bias & scale parameters for level-1b acc data (Version 2). Retrieved from http://podaac.jpl.nasa.gov/gravity/grace-documentation

Bettadpur, S. (2012). Gravity Recovery and Climate Experiment UTCSR Level-2 Processing Standards Document for Level-2 Product Release 0005, Center for Space Research, University of Texas, Austin, TX.

Bruinsma, S., Lemoine, J. M., Gegout, P., Biancale, R., & Bourgogne, S. (2014). *Updated release 3 of the GRACE gravity solutions from CNES/GRGS*. Abstract presented at the AGU Fall Meeting (G33A-0410), San Francisco, CA.

Chen, Q., Shen, Y., Chen, W., Zhang, X., & Hsu, H. (2016). An improved GRACE monthly gravity field solution by modeling the non-conservative acceleration and attitude observation errors. *Journal of Geodesy*, *90*(6), 503–523. https://doi.org/10.1007/s00190-016-0889-6

Chen, Q., Shen, Y., Zhang, X., Hsu, H., & Chen, W. (2015). Tongji-GRACE01: A GRACE-only static gravity field model recovered from GRACE level-1b data using modified short arc approach. *Advances in Space Research*, *56*(5), 941–951. https://doi.org/10.1016/j.asr.2015.05.034

Chen, Q., Shen, Y., Zhang, X., Hsu, H., Chen, W., Ju, X., & Lou, L. (2015). Monthly gravity field models derived from GRACE level 1b data using a modified short arc approach. *Journal of Geophysical Research: Solid Earth*, *120*, 1804–1819. https://doi.org/10.1002/2014JB011470

Dahle, C., Flechtner, F., Gruber, C., König, D., König, R., Michalak, G., & Neumayer, K. H. (2012). *GFZ GRACE level-2 processing standards document for level-2 product release 0005*. (Scientific Tech. Rep.-Data, 12). Potsdam: Deutsches GeoForschungsZentrum GFZ. https://doi.org/10.2312/GFZ.b103-1202-25

Desai, S. D. (2002). Observing the pole tide with satellite altimetry. *Journal of Geophysical Research*, *107*(C11), 3186. https://doi.org/10.1029/2001JC001224

Diedrich, R., & Gendt, G. (1989, August). *A gravity field model from LAGEOS based on point masses (POEM-L1)*. Proceedings of the 6th International Symposium "Geodesy and Physics of the Earth", Potsdam, Germany.

Ditmar, P., da Encarnação, J. T., & Farahani, H. H. (2012). Understanding data noise in gravity field recovery on the basis of inter-satellite ranging measurements acquired by the satellite gravimetry mission GRACE. *Journal of Geodesy*, *86*(6), 441–465. https://doi.org/10.1007/s00190-011-0531-6

Dobslaw, H., Bergmann-Wolf, I., Forootan, E., Dahle, C., Mayer-Gürr, T., Kusche, J., & Flechtner, F. (2016). Modeling of present-day atmosphere and ocean non-tidal de-aliasing errors for future gravity mission simulations. *Journal of Geodesy*, *90*(5), 423–436. https://doi.org/10.1007/s00190-015-0884-3

Drinkwater, M., Haagmans, R., Muzi, D., Popescu, A., Floberghagen, R., Kern, M., & Fehringer, M. (2006, November). *The GOCE gravity mission: ESA's first core Explorer*. Proceedings of the 3rd International GOCE User Workshop, Frascati, Italy.

Farahani, H. H., Ditmar, P., Klees, R., Liu, X., Zhao, Q., & Guo, J. (2013). The static gravity field model DGM-1S from GRACE and GOCE data: Computation, validation and an analysis of GOCE mission's added value. *Journal of Geodesy*, *87*(9), 843–867. https://doi.org/10.1007/s00190-013-0650-3

Flechtner, F., & Dobslaw, H. (2013). *AOD1B product description document for product release 05*. GFZ German Research Centre for Geosciences.

Flechtner, F., Neumayer, K. H., Dahle, C., Dobslaw, H., Fagiolini, E., Raimondo, J. C., & Güntner, A. (2016). What can be expected from the GRACE-FO laser ranging interferometer for Earth science applications? *Surveys in Geophysics*, *37*(2), 453–470. https://doi.org/10.1007/s10712-015-9338-y

Flury, J., Bettadpur, S., & Tapley, B. D. (2008). Precise accelerometry onboard the GRACE gravity field satellite mission. *Advances in Space Research*, *42*(8), 1414–1423. https://doi.org/10.1016/j.asr.2008.05.004

Folkner, W. M., Williams, J. G., & Boggs, D. H. (2008). The planetary and lunar ephemeris DE 421. JPL IOM 343R-08-003.

Förste, C., Bruinsma, S., Abrikosov, O., Flechtner, F., Marty, J. C., Lemoine, J. M., et al. (2014, May). *EIGEN-6C4—The latest combined global gravity field model including GOCE data up to degree and order 1949 of GFZ Potsdam and GRGS Toulouse*. EGU General Assembly, Vienna, Austria.

Golub, G. H., Heath, M., & Wahba, G. (1979). Generalized cross-validation as a method for choosing a good ridge parameter. *Technometrics*, *21*(2), 215–223. https://doi.org/10.1080/00401706.1979.10489751

Guo, J. Y., Shang, K., Jekeli, C., & Shum, C. K. (2015). On the energy integral formulation of gravitational potential differences from satellite-to-satellite tracking. *Celestial Mechanics and Dynamical Astronomy*, *121*(4), 415–429. https://doi.org/10.1007/s10569-015-9610-y

Harvey, N. (2016). GRACE star camera noise. *Advances in Space Research*, *58*(3), 408–414. https://doi.org/10.1016/j.asr.2016.04.025

Heiskanen, W. A., & Moritz, H. (1967). *Physical geodesy*. San Francisco, CA: Freeman.

Inácio, P., Ditmar, P., Klees, R., & Farahani, H. H. (2015). Analysis of star camera errors in GRACE data and their impact on monthly gravity field models. *Journal of Geodesy*, *89*(6), 551–571. https://doi.org/10.1007/s00190-015-0797-1

Jäggi, A., Beutler, G., Bock, H., & Hugentobler, U. (2007). Kinematic and highly reduced-dynamic LEO orbit determination for gravity field estimation. *Dynamic Planet*, 354–361. https://doi.org/10.1007/978-3-540-49350-1_52

Jäggi, A., Beutler, G., & Mervart, L. (2010). GRACE gravity field determination using the celestial mechanics approach—First results. In S. P. Mertikas (Ed.), *Gravity, Geoid and Earth Observation: International Association of Geodesy Symposia* (Vol. 135, pp. 177–184). Berlin, Heidelberg: Springer. https://doi.org/10.1007/978-3-642-10634-7_24

Klinger, B., & Mayer-Gürr, T. (2016). The role of accelerometer data calibration within GRACE gravity field recovery: Results from ITSG-Grace2016. *Advances in Space Research*, *58*(9), 1597–1609. https://doi.org/10.1016/j.asr.2016.08.007

Kurtenbach, E., Mayer Gürr, T., & Eicker, A. (2009). Deriving daily snapshots of the Earth's gravity field from GRACE l1b data using Kalman filtering. *Geophysical Research Letters*, *36*, L1710. https://doi.org/10.1029/2009GL039564

Kusche, J., Klemann, V., & Bosch, W. (2012). Mass distribution and mass transport in the Earth system. *Journal of Geodynamics*, *59*, 1–8.

Lemoine, F. G., Kenyon, S. C., Factor, J. K., Trimmer, R. G., Pavlis, N. K., Chinn, D. S., et al. (1998). *The development of the joint NASA GSFC and the National Imagery and Mapping Agency (NIMA) Geopotential Model EGM96*. (NASA Tech. Paper NASA/TP1998206861). Greenbelt, MD: Goddard Space Flight Center.

Liu, X., Ditmar, P., Siemes, C., Slobbe, D. C., Revtova, E., Klees, R., et al. (2010). DEOS mass transport model (DMT-1) based on GRACE satellite data: Methodology and validation. *Geophysical Journal International*, *181*(2), 769–788.

Mayer-Gürr, T. (2006). *Gravitationsfeldbestimmung aus der Analyse kurzer Bahnbögen am Beispiel der Satellitenmissionen CHAMP und GRACE* (PhD dissertation), University of Bonn, Germany.

Mayer-Gürr, T., Kurtenbach, E., Eicker, A., & Kusche, J. (2010). ITG-Grace2010 gravity field model. Retrieved from www.igg.uni-bonn.de/apmg/index.Php

Mayer-Gürr, T., Zehentner, N., Klinger, B., & Kvas, A. (2014, September). *ITSG-Grace2014: A new GRACE gravity field release computed in Graz*. Oral presentation at the GRACE Science Team Meeting Potsdam, Germany.

Meyer, U., Jäggi, A., Jean, Y., & Beutler, G. (2016). AIUB-RL02: An improved time-series of monthly gravity fields from GRACE data. *Geophysical Journal International*, *205*(2), 1196–1207. https://doi.org/10.1093/gji/ggw081

Pail, R., Goiginger, H., Mayrhofer, R., Schuh, W. D., Brockmann, J. M., Krasbutter, I., Höck, E., et al. (2010). GOCE gravity field model derived from orbit and gradiometry data applying the time-wise method. *Proceedings of the ESA Living Planet Symposium* (Vol. 28). ESA Publication SP-686, ESA/ESTEC.

Petit, G., & Luzum, B. (2010). *IERS conventions (2010)*. (IERS Tech. Note No. 36). France: Bureau International Des Poids et Mesures Sevres.

Rieser, D., Mayer-Gürr, T., Savcenko, R., Bosch, W., Wünsch, J., Dahle, C., & Flechtner, F. (2012). *The ocean tide model EOT11a in spherical harmonics representation* (Tech. Note, pp. 1–5). Retrieved from https://www.tugraz.at/fileadmin/user_upload/Institute/IFG/satgeo/pdf/TN_EOT11a.pdf

Savcenko, R., & Bosch, W. (2012). *EOT11a—Empirical ocean tide model from multi-mission satellite altimetry*. (DGFI Report No. 89).

Save, H. (2009). *Using regularization for error reduction in GRACE gravity estimation* (PhD dissertation). Austin, TX: University of Texas.
Schmidt, R., Flechtner, F., Meyer, U., Reigber, C., Barthelmes, F., Förste, C., et al. (2006). Static and time-variable gravity from GRACE mission data. *Observation of the Earth System From Space* (pp. 115–129). Berlin Heidelberg: Springer. https://doi.org/10.1007/3-540-29522-4_9
Seo, K. W., Wilson, C. R., Chen, J. L., & Waliser, D. E. (2008). GRACE's spatial aliasing error. *Geophysical Journal International*, *172*(1), 41–48. https://doi.org/10.1111/j.1365-246X.2007.03611.x
Shang, K., Guo, J., Shum, C. K., Dai, C., & Luo, J. (2015). GRACE time-variable gravity field recovery using an improved energy balance approach. *Geophysical Journal International*, *203*(3), 1773–1786. https://doi.org/10.1093/gji/ggv392
Shen, Y., Chen, Q., & Xu, H. (2015). Monthly gravity field solution from GRACE range measurements using modified short arc approach. *Geodesy and Geodynamics*, *6*(4), 261–266. https://doi.org/10.1016/j.geog.2015.05.009
Shen, Y., Xu, P., & Li, B. (2012). Bias-corrected regularized solution to inverse ill-posed models. *Journal of Geodesy*, *86*(8), 597–608. https://doi.org/10.1007/s00190-012-0542-y
Tapley, B. D., Bettadpur, S., Watkins, M., & Reigber, C. (2004). The gravity recovery and climate experiment: Mission overview and early results. *Geophysical Research Letters*, *31*, L09607. https://doi.org/10.1029/2004GL019920
Tapley, B. D., Flechtner, F., Bettadpur, S. V., & Watkins, M. M. (2013). *The status and future prospect for GRACE after the first decade*. Pasadena, CA: Jet Propulsion Laboratory.
Watkins, M. M., & Yuan, D. N. (2014). GRACE JPL level-2 processing standards document for level-2 product release 05.1, GRACE 327–744 (v 5.1).
Wiese, D. N. (2011). *Optimizing two pairs of GRACE-like satellites for recovering temporal gravity variations* (PhD dissertation). CO: University of Colorado at Boulder.
Wu, S. C., Kruizinga, G., & Bertiger, W. (2006). *Algorithm theoretical basis document for GRACE level-1b data processing V1. 2*. Pasadena, CA: Jet Propulsion Laboratory, California Institute of Technology. Retrieved from ftp://podaac.jpl.nasa.gov/allData/grace/docs/ATBD_L1B_v1.2.pdf
Xu, T., Ren, L., & Gao, R. (2017). Earth gravity field solution with combining CHAMP and GRACE data. *Geodesy and Geodynamics*, *8*(4), 246–252. https://doi.org/10.1016/j.geog.2017.03.016
Zehentner, N., & Mayer-Gürr, T. (2016). Precise orbit determination based on raw GPS measurements. *Journal of Geodesy*, *90*(3), 275–286. https://doi.org/10.1007/s00190-015-0872-7
Zhao, Q., Guo, J., Hu, Z., Shi, C., Liu, J., Cai, H., & Liu, X. (2011). GRACE gravity field modeling with an investigation on correlation between nuisance parameters and gravity field coefficients. *Advances in Space Research*, *47*(10), 1833–1850. https://doi.org/10.1016/j.asr.2010.11.041
Zhou, H., Luo, Z., Zhou, Z., Zhong, B., & Hsu, H. (2017). HUST-Grace2016s: A new GRACE static gravity field model derived from a modified dynamic approach over a 13-year observation period. *Advances in Space Research*, *60*(3), 597–611. https://doi.org/10.1016/j.asr.2017.04.026